Sedimentary stylolite networks and connectivity in Limestone: Large-scale field observations and implications for structure evolution

Leehee Laronne Ben-Itzhak, Einat Aharonov, Ziv Karcz, Maor Kaduri, Renaud Toussaint

Sedimentary stylolite networks and connectivity in Limestone: Large-scale field observations and implications for structure evolution

Laronne Ben-Itzhak L.[1], Aharonov E.[1], Karcz Z.[2,*],
Kaduri M.[1,**] and Toussaint R.[3,4]

[1] *Institute of Earth Sciences, The Hebrew University, Jerusalem, 91904, Israel*

[2] *ExxonMobil Upstream Research Company, Houston TX, 77027, U.S.A*

[3] *Institut de Physique du Globe de Strasbourg, University of Strasbourg/EOST, CNRS, 5 rue Descartes, F-67084 Strasbourg Cedex, France.*

[4] *Centre for Advanced Study at The Norwegian Academy of Science and Letters, Drammensveien 78, 0271 N-Oslo, Norway.*

[*] *Currently at Delek Drilling LP*

[**] *Currently at ISTerre, University J. Fourier – Grenoble I, BP 53, F-38041 Grenoble, France*

Abstract

Stylolites are rough surfaces, formed by localized rock dissolution, and prevalent in carbonates and other sedimentary rocks. Their impact on porosity and permeability, and capacity to accommodate compactive strain, are well documented. This paper presents a meso-scale field study on sedimentary stylolites in carbonates, characterizing large-scale distributions of stylolites, including measurements conducted on longer than kilometer-long stylolites. Our field study suggests that on large-scales connections between stylolites become important. Since connectivity, and also lack of connectivity, are expected to play a significant role in strain accommodation and hydraulic rock properties, we suggest that large-scale analysis may require a new characterization scheme for "stylolites populations", based on their connectivity. We therefore divide sedimentary stylolite populations into three end-member types, which are correlated with the three possibilities for percolation of such systems: isolated stylolites (with zero percolation/connectivity), long-parallel stylolites (with 2-dimensional percolation/connectivity), and interconnected stylolite networks (with 3-dimensional percolation/connectivity). New statistical parameters and measures are devised and used to quantitatively characterize the different population types. Schematic mechanistic models are then offered to explain the evolution of the three end-member connectivity-classes. In addition we discuss the effect on fluid flow of the different population types.

1. Introduction

Stylolites are rough surfaces of dissolution, common in sedimentary rocks and especially prominent in carbonates. They are lined by a thin layer of relatively insoluble particles, mainly clay minerals, oxides, and organic matter, that are thought to accumulate while the major constituent of the rock, which is more soluble (e.g. carbonate, quartz) dissolves away (Stockdale, 1922, Park and Schot, 1968, Kaplan, 1976, Railsback, 1993). Stylolites are known to affect fluid flow in opposing ways: On the one hand, stylolites are often associated with reduced permeability - material that dissolves at the stylolite precipitates in adjacent pores, forming "tight" units (Wong and Oldershaw, 1981, Tada and Siever, 1989, Finkel and Wilkinson, 1990, Ehrenberg, 2006) that are important in management of hydrocarbon aquifers and reservoirs (Corwin et al., 1997). In other cases, stylolites may enhance porosity and permeability in their vicinity, in particular their tips (Carozzi and Vonbergen, 1987, Raynaud and Carrioschaffhauser, 1992) and sometimes fluid flow is observed along stylolitic surfaces (Wong and Oldershaw, 1981, Rye and Bradbury, 1988, Heap et al., 2014). In addition to their hydraulic role, stylolites are also known to accommodate large compactive strains (Tada and Siever, 1989), playing a key role in the evolution of mechanical rock properties, and the overall compactive strain of rocks.

Stylolite formation is attributed to localized Pressure Solution (PS). PS is broadly defined as dissolution and re-precipitation driven by spatial variations in chemical potential along grain surfaces: regions with high chemical potential dissolve, the dissolved material is transported through the fluid phase, and precipitates in regions where the chemical potential is lower. Variations in the chemical potential arise due to spatial variations in stress, plastic and elastic strain energies, crystal orientation and interface curvature (Deboer, 1977, Lehner, 1995, Paterson, 1995, Shimizu, 1995). The chemical potential can be extended to an electrochemical

potential (Greene et al., 2009) where spatial variations in surface charge are considered as well. Clays and organic matter are also thought to play an important role in the PS process (Heald, 1956, Thomson, 1959, Sibley and Blatt, 1976, Gruzman, 1997), and their distribution and content are believed to affect the rate of PS (Hickman and Evans, 1995, Renard et al., 2001) and the degree of PS localization on stylolites (Heald, 1955, 1956, Engelder and Marshak, 1985, Marshak and Engelder, 1985). How clays, phyllosilicates, and organic matter enhance PS is not fully understood, and suggestions include purely physical (propping grain contacts) (Weyl, 1959), chemical (varying pH) (Thomson, 1959), electrochemical (solute gradients amplified by clay electric charge) (Walderhaug et al., 2006) effects, or a combination of the above.

Key models for stylolite formation view them as isolated and spatially limited surfaces (e.g. Fletcher and Pollard (1981); Stockdale (1922)). However, in the field they are rarely “isolated”, but rather appear to be closely related to other stylolites and structures (primarily Mode I and Mode II fractures) (Peacock and Sanderson, 1995, Smith, 2000). Perhaps because of the scarcity of isolated stylolites, and the difficulty in determining their terminations when not isolated, there is very limited literature on stylolites' lateral extent. Stylolites were traced in limestone for over 50 m by Park and Schot (1968), and Safaricz (2002) followed single stylolites for 8.5m and dissolution seams for over 800 m. An often-cited linear relationship between stylolite length and thickness (either amplitude or seam thickness), is thus based on a handful of field studies (Stockdale, 1922, Mardon, 1988, Benedicto and Schultz, 2010, Nenna and Aydin, 2011) though a theoretical rationale for it is fairly well understood (Aharonov and Katsman, 2009).

Most stylolites seem to have been studied on "small" outcrops or, in the case of the oil and gas industry, on cores. A few exceptions are the field-wide studies of (Stockdale, 1922, Railsback, 1993, Andrews and Railsback, 1997, Safaricz, 2002, Safaricz and Davison, 2005). Stylolites, like fractures, are "very large" in one dimension but "very small" in another dimension. Their thickness is of the order of centimeters at most, so they are impossible to resolve with standard seismic techniques. In order to determine the large-scale distribution of

stylolites (needed to assess for example reservoir performance or compactive basin-scale strain) the geometry and hydraulic properties of the centimeter-scale observation made routinely on cores needs to be upscaled to the kilometer-scale structure, which is always a challenging task. To devise a robust upscaling methodology, the cm-scale structure needs to be linked to the km-scale structure through an adequate analog-outcrop, as is common in the petroleum industry. Only through such an analog can upscaling parameters and workflows be tested and confirmed. Such studies were previously done on fractures (Dawers et al., 1993, Main, 1996, Cello, 1997, Willemse, 1997, Bour and Davy, 1998, McLeod et al., 2000), and led to basic understanding regarding the relationship between aperture and length (Vermilye and Scholz, 1995) and the formation and connectivity of fractures (Segall and Pollard, 1980, Cartwright et al., 1995, Gupta and Scholz, 2000). The present work performs a similar multi-scale study on sedimentary stylolites populations, aiming to quantify their distributions and connectivity and provide a step towards understanding their large-scale effects.

The connectivity of stylolites may be important both when they act as flow conduits, and in the opposite case, when they act as barriers. Their impact on large-scale flow properties can be understood using ideas from percolation theory (for a review on percolation see e.g. Bunde and Havlin (1991)). Percolation theory is a mathematical theory that addresses the question of the connectivity and conductivity within a composite material, composed of "black" defects placed within a "white" matrix. In the percolation "game" the black defects are typically assigned a different conductivity than their host white matrix, and percolation theory predicts electrical conductivity and resistivity of the composite black-white material (e.g. McLachlan et al. (1990)). The black defects are said to "percolate" when one can trace along black parts only (without "stepping" into white parts) from any side of the matrix body to any other. When black defects are conductive "percolation" is accompanied by abrupt enhancement of the conductivity of the matrix relative to a state of no percolation. The opposite game is just as simple – if black defects

have high resistivity (low conductivity), percolation of conducting whites controls conductivity. Percolation of conduction whites is lost when there are enough black defects, or when blacks are distributed in such a way that whites are disconnected.

In line of the above percolation picture, we suggest to envision stylolites as "penny-shaped" surfaces with a different fluid conductivity (higher or lower) than their host rock. These surfaces can have different radii and they can be oriented in different angles to each other and can be envisioned as "black" defects in a "white" host rock.

Percolation or connectivity of the stylolite surfaces are then expected to occur in one of three end-member ways:

I: Isolated surfaces – no percolation: If the radii of surfaces is small, and if there are not many surfaces within the region, then the surfaces may not cross each other and remain isolated from one another. In that case there is no percolation of surfaces from any side of the box to any other. This system is below the percolation threshold.

II: Parallel surfaces - 2D percolation: if surfaces are virtually infinite and parallel, they create a layered structure. In this case both surfaces and host rock percolate in the direction parallel to the surfaces, but neither of them percolates in the direction perpendicular to the surfaces. If the surfaces have higher conductivity than the host rock they will enhance conductance in the surface-parallel direction and will not affect the perpendicular direction. Instead, if the surfaces have lower conductivity they will not affect the surface-parallel direction yet will act as barriers for conductance in the perpendicular direction. In this case percolation is anisotropic and so is conductance.

III: Networks of interconnected surfaces - 3D percolation: when there are enough surfaces, and they have a distribution of orientations, they will connect to one another and allow percolation in all three dimensions.

In order to analyze the 3D connectivity of stylolites with the above framework in mind we devised new statistical characterization tools that quantify the morphology of stylolite populations. We use our new tools in three well-exposed localities, chosen from a collection of 17 field-sites (Table 1). These sites were chosen due to their good exposure, and also because they exemplify the 3 end-member surface-connectivity/percolation possibilities presented above. The Supplementary provides location, geological setting and general description of stylolites exposed in the other 14 localities. Most of these are field-sites that we studied and a few are places described in the literature and studied by others.

2. Methods

2.1 Field sites

Three well-exposed "type" localities (1-3 in Table 1) that display possible connectivity end-member behaviors were chosen out of 17 sites (see the Supplementary Material). Detailed measurements were made in these three localities. A Bedding-parallel population of very long stylolites is studied in the Blanche cliff site to represent 2D percolation. To represent 3D percolation an anastomosing network of stylolites is analyzed in the Mitzpe Ramon quarry and a more complicated case, with a *stylolite-fracture network* that has also several *long-parallel stylolites* was investigated on an Umbria-Marche slab. *Isolated stylolites,* representing a non-percolating population, were not found in our field sites (as seen in Table 1). Their scarcity is explained in the discussion, while here this connectivity class is discussed based on few examples from the literature, because topologically it is an end-member scenario, even if not commonly found in the field. The three key field localities we study are described in detail below, while the other sites are referred to in the Supplementary Material.

Table 1: Field locations, which were studied as part of this work (1-13) and collected from the literature (14-17). Detailed description and photographs are presented in the text and in the Supplementary material. Class II: Long-parallel stylolites, Class IIIa: Anastomosing stylolite network, Class IIIb: stylolite-fracture network

#	Site	Location	Geological data	Population class
1	Blanche cliff	N33°12' E35°33'	Ein-El-Assad Formation (Albian), biomicritic limestone	II
2	Mitzpe Ramon (quarry) (unit U1)	N30°38' E34°48'	Avnon formation (Upper Cenomanian), bioclastic limestone.	IIIa
3	Umbria-Marche, Italy, (purchased slab)	N43° E13°	Calcare Massiccio (CM) Formation (Lower Jurassic). Wackestone–packstone limestone.	IIIb + several II
4	Mitzpe Ramon (quarry) 4 units (other than unit U1)	N30°38' E34°48'	Avnon formation (Upper Cenomanian), bioclastic limestone.	Different units: 1 unit contains IIIb , and 3 units of IIIa.
5	Nahf (quarry)	N32°56 E35°19'	Bina formation (Turonian).	II with IIIa appearing in between
6	Ein El-Assad (cliff)	N32°56' E35°23'	Ein-El-Assad Formation (Albian).	II with IIIa appearing in between
7	Tsavoa anticline (roadcut)	N30°58' E34°46'	Nezer Formation (Turonian), biomicritic limestone interlayered with dolomite and marl	II (some connections at large scales)
8	Rama (cliff)	N32°56' E35°21'	Rama Formation (Albian), limestone interlayered with marl.	IIIa
9	Machtesh Katan (exposure)	N30°57' E35°13'	Shivta and Nezer formations (Turonian)	IIIb
10	Maale Yair, Dead Sea (exposure)	(N31°12' E35°21')	Shivta formation (Turonian)	IIIa
11	State Collage, Pennsylvania (roadcut)	(N40°47' W77°48')	Devonian-Silurian limestone	II
12	Morocco (exposure)	??	??	II
13	Givat Ram, Jerusalem		Cenomanian (?), limestone	IIIa with some localities of IIIb
14[1]	Flamborough Head, Yorkshire, UK	between Sewerby / Bridlington and High Stacks	Cretaceous chalk	IIIa and II
15[2]	Yazd Block quarry, Esfahan Province, Central Iran	(N33°27' E54°22')	Haftoman Formation (Upper Cretaceous), limestone	IIIa
16[3]	Illinois Basin Salem Limestone	Two coadcuts: N38°53' W86°31' and N38°32' W90°24'	Mississippian Salem limestone	II and IIIa
17[4]	Selinsgrove Junction, Pennsylvania (creek bed exposure)	N40°47' W76°50'	Selinsgrove member, Onandaga fm (Devonian), fine-grained limestone	tectonic isolated as well as networks of ("composite-") solution seams

Blanche cliff (Fig 1): Stylolites are exposed in the “Blanche” cliff of the Albian-age Ein-El-Assad Formation in Northern Israel. The "Blanche" here consists of a ~50m-thick biomicritic, shallow inner-platform limestone, that dips gently to the west (Sneh and Weinberger, 2003). It contains well-developed (cm-scale teeth amplitudes) bedding-parallel stylolites, which can be traced for the full extent of the outcrop, i.e., more than 1km. These are, as far as we know, the longest measured stylolites reported in the literature. Roughness of these stylolite surfaces was measured and analyzed by us in a previous paper (Laronne Ben-Itzhak et al., 2012), and is characterized by a Hurst exponent H~0.65, and by an upper cutoff for self-affinity at around 50cm. In the lowermost part of the section some interconnected stylolite networks were observed between the long parallel stylolites.

Mitzpe Ramon Quarry (Fig 2): In this quarry near the town of Mitzpe Ramon in Southern Israel, networks of interconnected stylolites appear in massive, subhorizontally stratified, bioclastic limestone of the Upper Cenomanian Avnon Formation. This site provides 3D exposures over tens of meters of polished quarry walls. The exposures consist of several vertical units that differ in stylolites networks’ characteristics and in the presence or absence of fractures. In the unit of focus, where fractures are not common, the stylolites do not terminate *per se*, but rather connect to each other, so that stylolites can be traced from one side of the outcrop to any other side. In such networks stylolites delineate ‘islands’ or „lenses’ of non-dissolved rock, as seen in Fig 3 (see site #4 in Supplementary A and in Table 1 for details on other units in this location).

Umbria–Marche slab, Apennines: (Fig 4): This is a 3-m-long, 1.2-m-wide and 2-cm-thick limestone slab of the Calcare Massiccio (CM) Formation (Lower Jurassic) of the Umbria–Marche of Central Italy. The slab is a wackestone–packstone limestone. The Roughness of the major stylolites (i.e. a subset of the population, defined below) exposed here was studied by Karcz and Scholz (2003) and was found to be fractal over 4.5 orders of magnitude (with a Hurst exponent of ~0.5). In this site stylolites and veins form various interconnecting geometries.

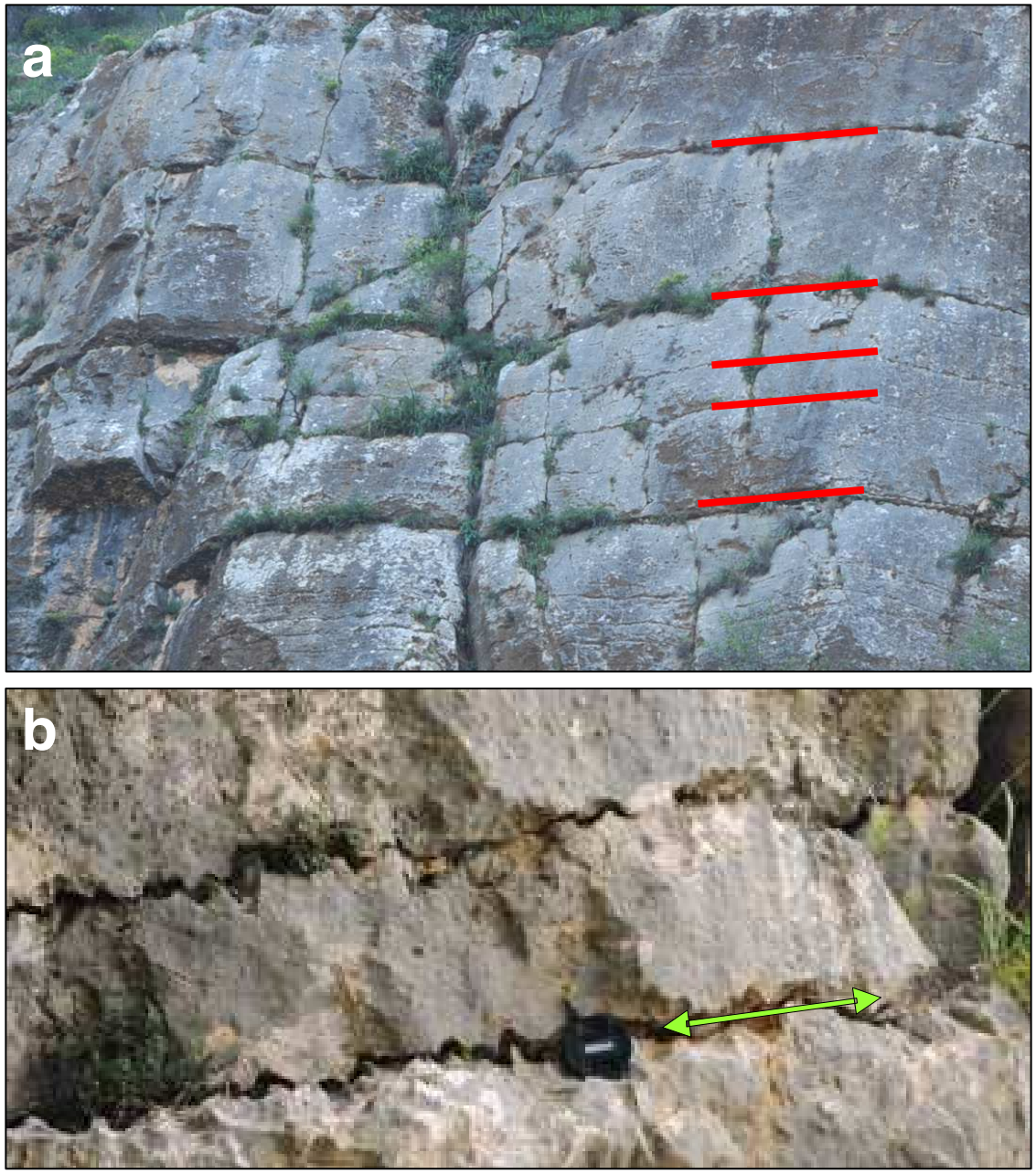

Fig 1: Long parallel stylolites in the Blanche cliff, Northern Israel.

(a) Part of the cliff with four stylolites (labeled '4(19)', '5(7)', '5(9)' and '5(13)' in Figure 5b) marked in red, showing they can be traced for a large distance.

(b) Zoom on two other stylolites ('3(10)' marked by a green arrow, and '3(11)', see Figure 5b), where stylolite cm-scale roughness is evident.

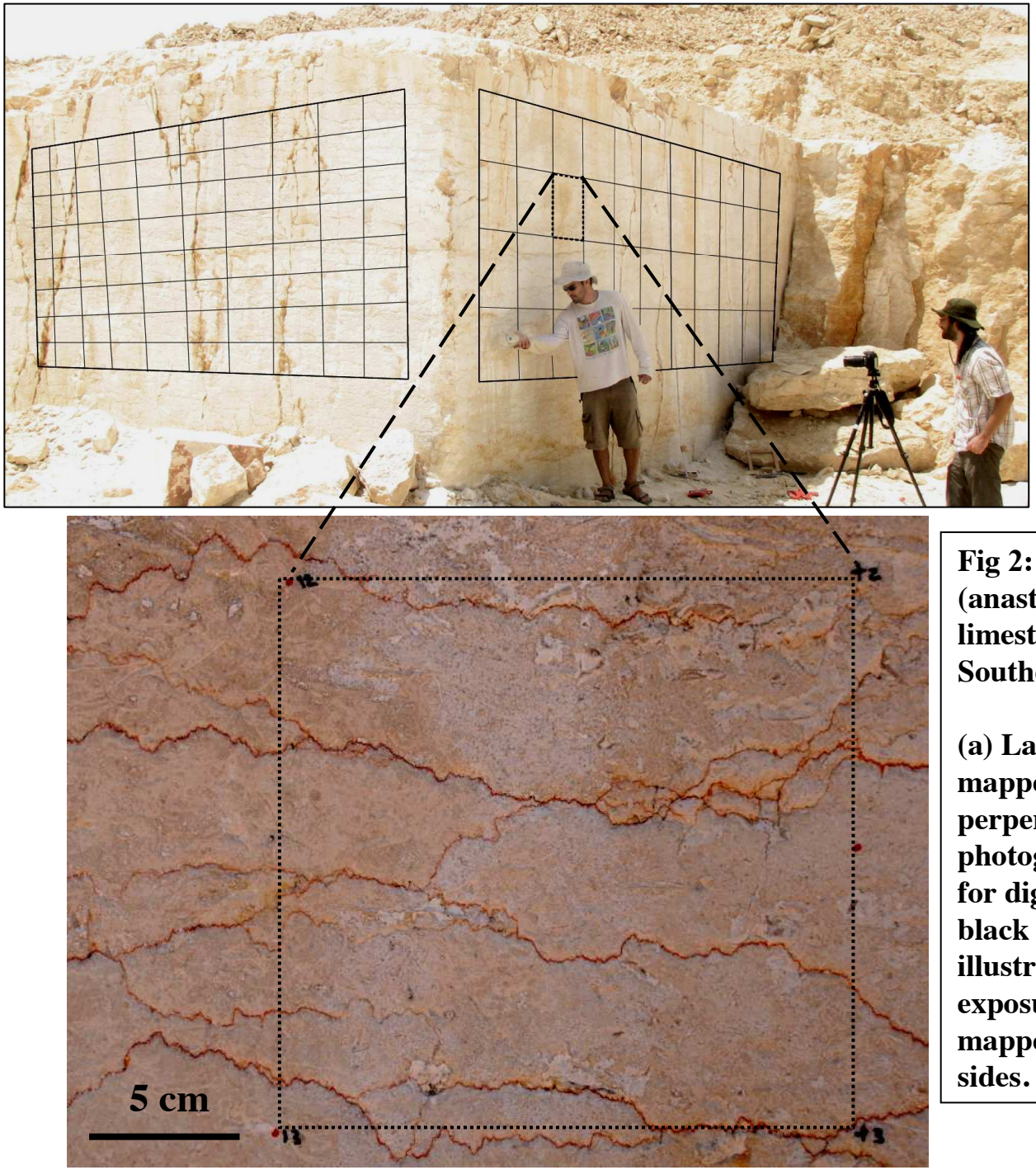

Fig 2: Interconnected stylolite network (anastomosing) from a Cenomanian limestone quarry near Mitzpe Ramon, Southern Israel.

(a) Large scale photo and (b) zoom of the mapped exposure, studied from two perpendicular sides. High-resolution photographs were combined using a grid for digitization of the stylolite network (the black grid in (a) was drawn on the photo to illustrate where the actual grid on the exposure was marked). 5.5 x 1.2 m^2 were mapped on either of the two perpendicular sides.

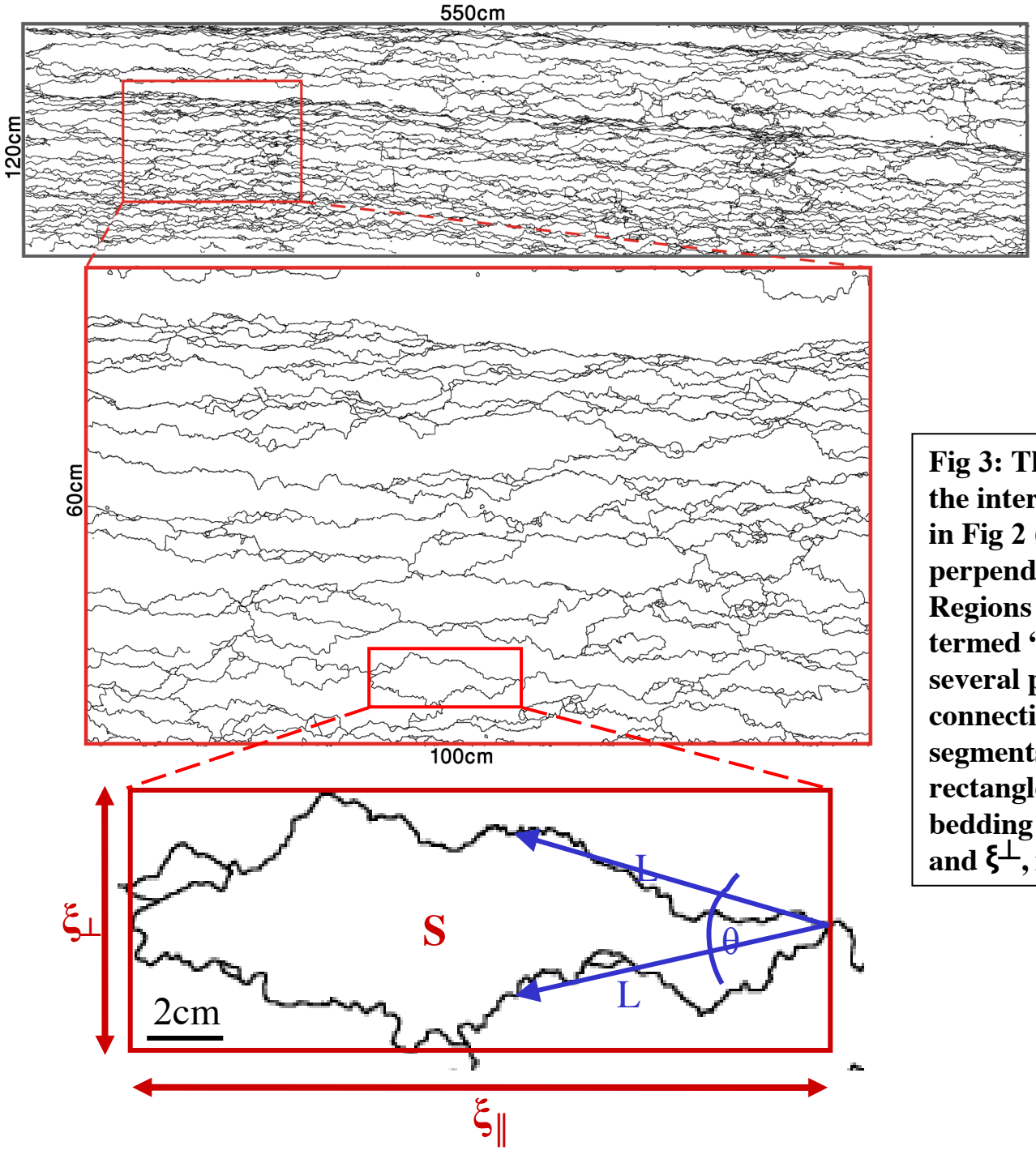

Fig 3: Three scales of a digitized map of the interconnected stylolite network seen in Fig 2 (the right section of the two perpendicular exposures in fig 2). Regions between connected stylolites, termed "islands", are described by several parameters: island area S; connection angle θ between stylolite segments of length L; and a bounding rectangle with bedding-parallel and bedding perpendicular dimensions ξII and $\xi^{\perp}$, respectively.

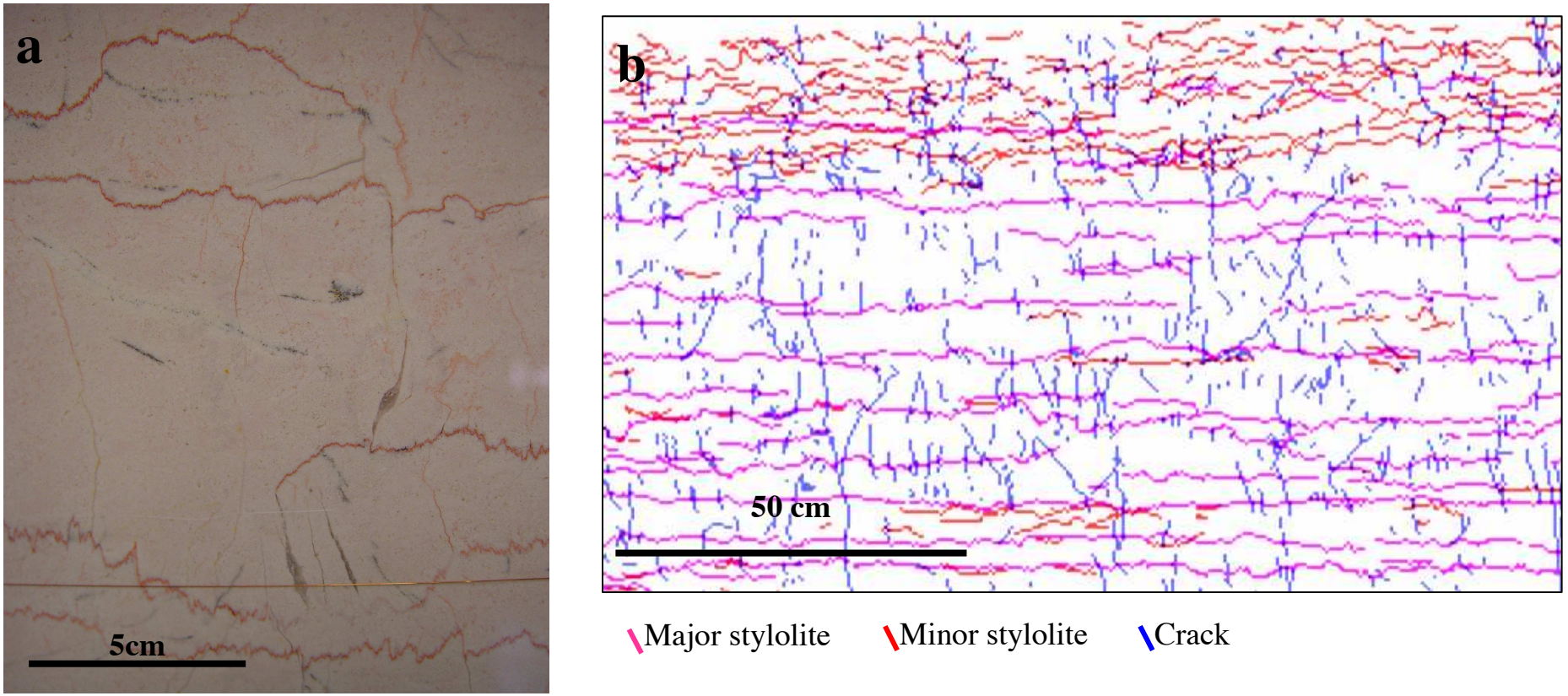

Fig 4: Interconnected network of stylolites and fractures in limestone (Calcare Massiccio Formation, Jurassic, Italy).

(a) photo; and

(b) digitized map of major and minor stylolites (pink and red, respectively) and of fractures (blue).

197

198 **2.2 Description of measurements**

199 The type of measurements conducted on the various stylolite populations and their resolution
200 was tailor-fit to the population characteristics.

201 *Long parallel populations* –stylolitic roughness was previously analyzed in this cite in order
202 to study the amount of dissolution on them (Laronne Ben-Itzhak et al., 2012). Here we look at
203 different characteristics of the same stylolites, namely lateral variations in maximum stylolite
204 amplitude (A_{max}) and in spacing between them (d). These characteristics were chosen in order to
205 establish uniformity in bedding parallel direction and connectivity in 2D. At the Blanche cliff all
206 observable stylolites (a total of 65 stylolites) were measured at the northern part of the cliff (Fig
207 5). The cliff was then divided into 9 units, separated by prominent stylolites. Each stylolite was
208 named according to its position in the unit (for example: stylolite '3(10)' is the 10th stylolite in
209 unit 3). Six specific stylolites („3(10)', „3(11)', „4(18)', „4(19)', „5(7)' and „5(9)') that are easily
210 viewed and are accessible at least in some places along the cliff, were traced and measured in
211 several stations along the exposure. Spatial measurements were done directly on the cliff using a
212 tape, or, where access was difficult, on digital images. Since stylolites are fractal surfaces (Karcz
213 and Scholz, 2003, Renard et al., 2004, Schmittbuhl et al., 2004, Ebner et al., 2009b), properties
214 such as mean and maximum amplitude depend on the scale of observation, l. Therefore A_{max} was
215 defined here as the maximum distance from peak to crest along l=1m length (based on Laronne
216 Ben-Itzhak et al. (2012)).

217

218 *Anastomosing networks* In this type of population islands of rock are captured and become
219 isolated between stylolites, while stylolites meet, join, and percolate in all directions. Such
220 systems are somewhat more complex to characterize than long parallel stylolites. For example,
221 both stylolite amplitudes and spacing are ill-defined in anastomosing networks. We thus chose to

222 characterize such networks via (as defined in Fig 3): a) connection angle (θ) between stylolites
223 and b) the dimensions of "islands" demarcated by stylolites. At the Mitzpe Ramon site, the 10m
224 columnar section was studied at several locations in the quarry and was then divided into 5 units,
225 characterized by different density of the stylolite network, different fossils, and presence or
226 absence of fractures (Kaduri (2013), and see also supplementary A). We chose to focus on one of
227 these units, in which fractures and veins are rare and which does not contain large fossils. To
228 obtain connection angle and island dimensions for the entire network, the stylolites in this unit
229 were digitized from digital images (200μm resolution) to yield two perpendicular maps (550x120
230 cm each, Fig 3). The digital maps were then saved as grids composed of squares colored black
231 for stylolites or white for rock (Fig 3c). The black and white maps were analyzed using image-
232 processing tools in MatLAB and MatLAB codes written in Kaduri (2013) to obtain:
233 1. Values of connection angle θ measured between each two connecting stylolite lines, as a
234 function of the distance L from their meeting junction, as defined in Fig 3.
235 2. In order to obtain island dimensions, regions between stylolites ("islands") were digitally
236 identified, and each of the islands given a serial number. In this way more than 3000 islands were
237 obtained. Each island was then bound by a rectangular box (a "bounding box"), with horizontal
238 and vertical lengths ξ_{II} and $\xi_{\perp}$, respectively (as depicted in Fig 3), to provide an estimate of their
239 lateral and vertical dimensions. The scaling behavior of the networks may be partially revealed
240 by studying the dependence between ξ_{II} and $\xi_{\perp}$ for each island. Similar analysis was performed
241 on fluid cluster populations in two-phase flow in porous media (Tallakstad et al., 2009a,
242 Tallakstad et al., 2009b) and on networks of propagating fracture fronts, to extract the statistics
243 of rupture avalanches (Maloy et al., 2005, Maloy et al., 2006, Tallakstad et al., 2011).
244
245 *Stylolite-fracture networks.* The stylolites and fractures in the network of the third site were
246 digitized on the slab at a 0.5mm resolution. This type of network is composed of long, sub-
247 parallel stylolites, which extend from one side of the slab to the other (termed here "major"

248 stylolites), and shorter (defined here as "minor") still sub-parallel, stylolites (Fig 4b). In addition
249 the network is composed also of fractures that illustrate geometrical interactions with stylolites,
250 as shown below. Orientations of stylolites and of fractures were studied statistically, and
251 qualitative descriptions of interactions between fractures and stylolites were made, in order to
252 constrain the mechanical evolution of this network and its associated strain.
253

254 ## 3. Results and data analysis

255

256 The measurements conducted in the three key field-sites are presented here by site.
257

258 ### 3.1 Long-parallel stylolites in the Blanche cliff

259 A crucial finding in the Blanche cliff site (and in sites #5, 6, 7, 11 and 12 shown in the
260 Supplementary Material) is that most stylolites are as long as the ~1km outcrop and are parallel
261 to each other and to the bedding. No fractures or joints related to the stylolites were observed and
262 the major faults, which terminate the exposure on both sides, are post-stylolitization. Two
263 variables were measured along the cliff exposure to detect spatial variations: spacing between
264 adjacent stylolites (d, defined in Fig 5), and maximum teeth height of individual stylolites (A_{max}).
265 Although d ranges from 0.1 to 2.0 meters when looking at different neighbors, the spacing
266 between any two given stylolites is laterally constant, as seen qualitatively in Fig 1 and as
267 quantitatively measured over ~1km in Fig 6a. For example, d between stylolites 3(10) and 3(11)
268 varies (without any obvious spatial trend) between 15 and 22 cm along 850m of the exposure.
269 The lateral variation of maximum stylolite amplitude (A_{max}) in the Blanche cliff shows no
270 particular trend, i.e. it does not decrease or increase gradually in any direction (Figs 6b, 6c). For
271 example, A_{max} of stylolite 3(10) varies between 2.5 and 5.5 cm, which in itself may be
272 significant, but does not vary consistently in any direction (e.g. from the center of the cliff

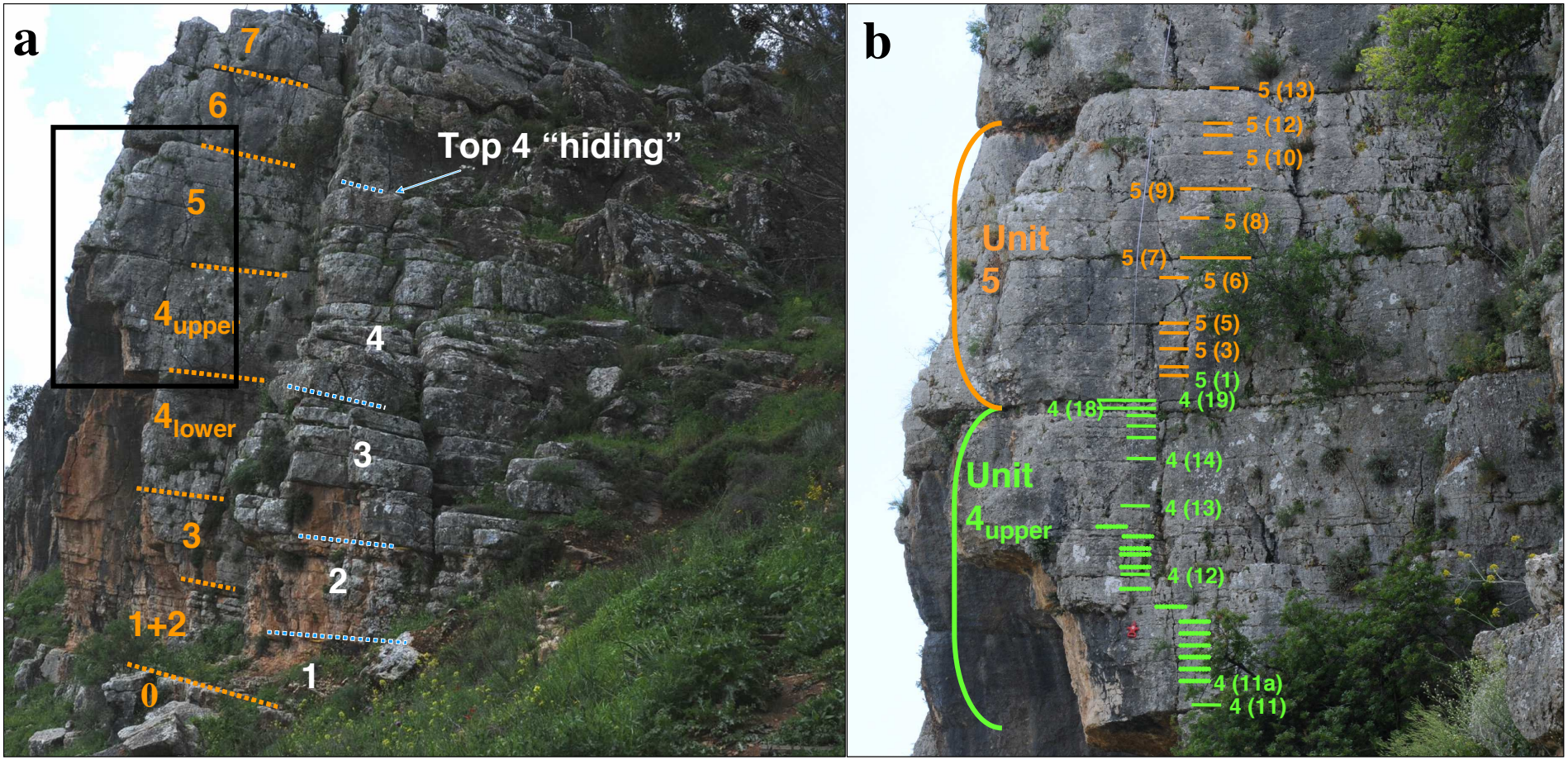

Fig 5: Images showing the Blanche (Ein El-Assad Fm.) section in the northern part of the cliff, where all 65 stylolites were identified and measured.

(a) **The section was divided to 9 major units differentiated by major stylolites (in orange). Most of the measurements were performed in the parts that are marked in white, which are more accessible.**

(b) **Zoom on rectangle in (a). Stylolites are labeled according to their vertical position within a unit, i.e., 5 (3) is the third stylolite from the bottom of unit 5.**

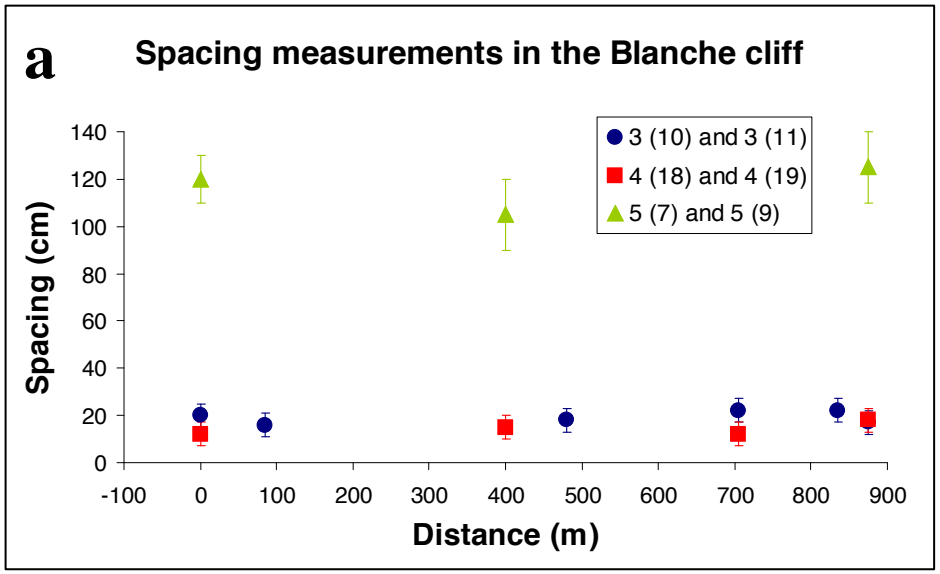

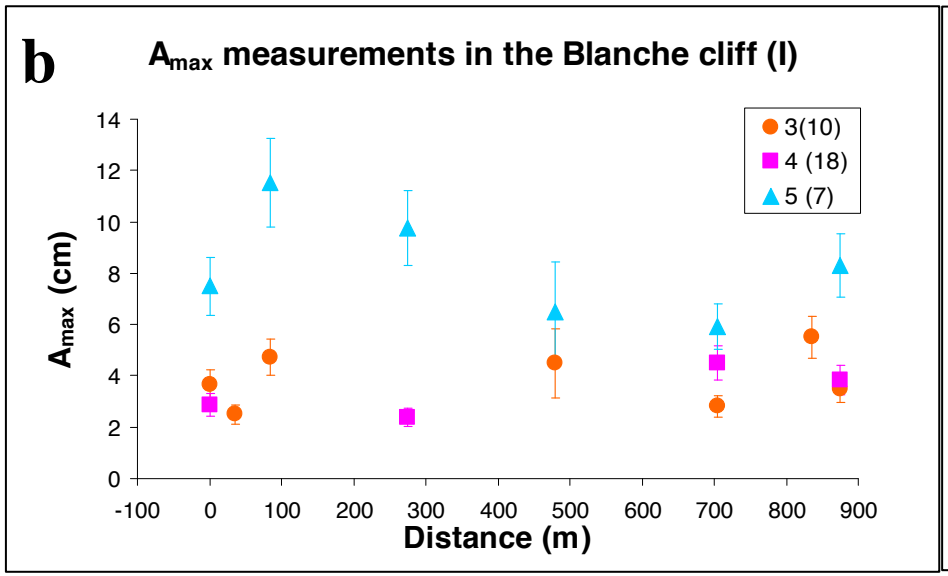

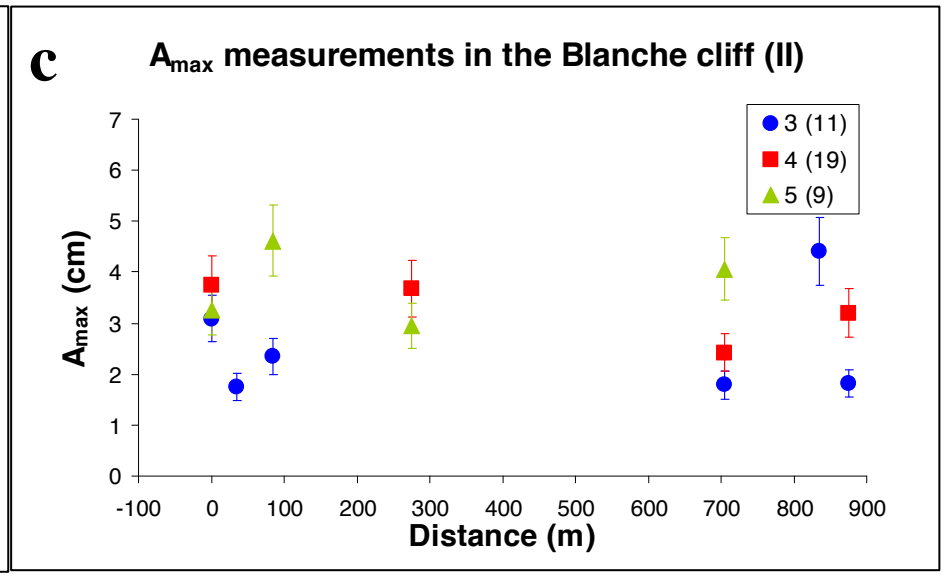

Fig 6: Measurements conducted on long parallel stylolites at several locations along the ~1km – long Blanche cliff.

(a) Spacing between three couples of stylolites.

(b) and (c) Maximum teeth amplitude (A_{max}) of six different stylolites (viewed in two separate graphs only for purposes of convenience). Error bars are the standard deviation of several measurements in each location. No trend in spacing or A_{max} along the length of the stylolites is identified.

sideways, or from one end to the other). This either suggests that terminations are still far away, or that the observations and conclusions of Mardon (1988) and Stockdale (1922) on isolated seams, showing tapering of seam thickness and teeth amplitude from center to edges, do not apply here. This will be discussed below.

3.2 Anastomosing stylolite network in Mitzpe Ramon Quarry

We focus here on statistics of islands formed by stylolites. The islands vary widely in size, from centimeter to a couple of meters in width and length, yet show robust characteristics: Fig 7a shows the connection angle, θ, between two connecting stylolites, as a function of the distance from their junction, L, as defined in Fig 3. Each data point is the average of all $\theta(L_i)$ in the exposure and the error bars are the standard deviation, both produced from normal distribution best-fits to each value of L (inset in Fig 7a). Connection angle in the anastomosing stylolite network of the Mitzpe Ramon Quarry is found to be distance dependent. Close to the connection points, i.e. for L<2cm, θ=80º-90º, but this value decreases asymptotically to zero (stylolites become sub-parallel) for larger values of L. This means that stylolites meet at near perpendicular angles (similarly to cracks), but approach parallel planes when far "enough" apart (L>>5cm).

Fig 7b shows vertical versus horizontal dimensions ($\xi_\perp$ versus ξ_{II}), of over 3300 islands analyzed in this site. We identify a robust power-law relation between the height and width of islands: Performing a linear fit in bi-logarithmic space of $\xi_\perp$ versus ξ_{II} , we obtain

(1) $\xi_\perp = k\xi_{II}^{\alpha}$

with k [$m^{1-\alpha}$] =0.67 ± 0.01 and α (unitless) = 0.67 ± 0.03 (The reason that both constants are equal is probably by chance).

Fig 7:
Results of the statistical analysis performed in Mitzpe Ramon quarry.

(a) θ(L) and

(b) Island dimensions, as explained in the text.

The variables are illustrated in Fig 3c. Each data point in (a) is the average of all θ(Li) in the exposure and the error bars are the standard deviation.
The pink line in (b) is a best fit to the correlation between $\xi_{\perp}$ and ξ_{II} with both α and k equal 0.67.

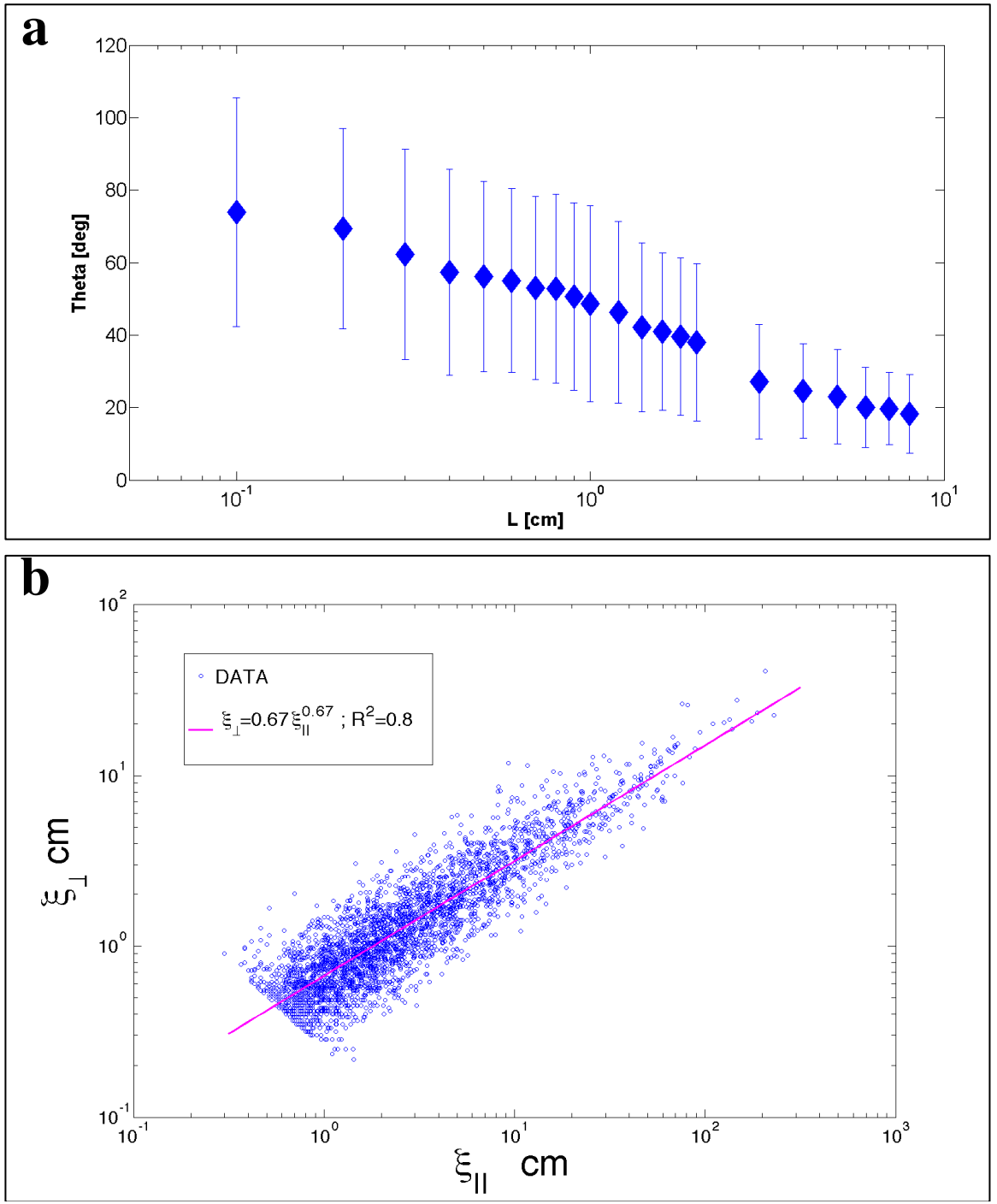

3.3 Stylolite-fracture network in the *Umbria–Marche* slab, Apennines

We view the major stylolites of this slab (Fig 4b) as a long-parallel population (shown to be fractal over 4.5 orders of magnitude (Karcz and Scholz, 2003)), whereas the minor ones are either anastomosing, connected to fractures, or isolated. Many of the fractures have clear interactions with the stylolites, e.g. emanating from-, or connecting between- stylolite tips, or emanating from stylolite teeth. Stylolites and fractures are found to be generally perpendicular to each other, as seen qualitatively in Fig 4b and quantitatively in Fig 8. However, a significant population of fractures that are sub-parallel to the stylolites is also seen in Fig 8.

Small-scale observations

Relations between stylolites and fractures in this network imply that the two types of features are probably related to one another (Fig 9). Stylolites are often connected to each other via fractures (Figs 9a, 9d, and 9f), though regions of anastomosing stylolites are also quite common (Fig 9c). Fractures in this network are either Mode I veins or Mode II shear fractures with some offset. Fractures interpreted as Mode II shear fractures based on geometrical considerations, may exhibit small "pull-apart" features filled with cement (Fig 9a). Many Mode I veins appear at some acute angle to stylolites while others emanate from stylolite teeth (or what seem to be terminations) and are perpendicular to the stylolite mean surface (Fig 9b). Veins connected to stylolites often taper away from the stylolite (e.g. Fig 9b). Similar tapering was also described by Eren (2005). Some fractures simply connect neighboring stylolites (Figs 9a, 9f) while complex connections, such as in Fig 9d, are very common as well. At the scale of observation, some features appear not to be fully physically connected (e.g. Figs 9b, 9d). Perhaps there is connection in 3D that is not seen in the 2D view. Even when the connections are more difficult to observe, such as in Fig 9b, geometry suggests strain-related interactions between the stylolites and fractures.

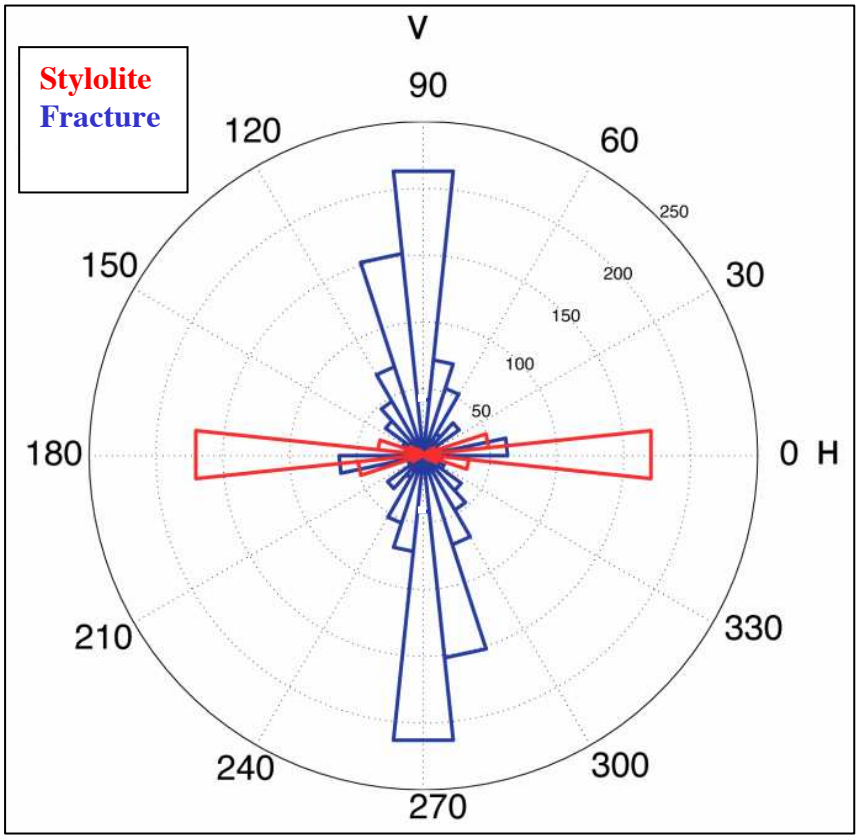

Fig 8: Orientations of stylolites and fractures in the Umbria–Marche slab, Apennines (analyzed upon map in Fig 4).

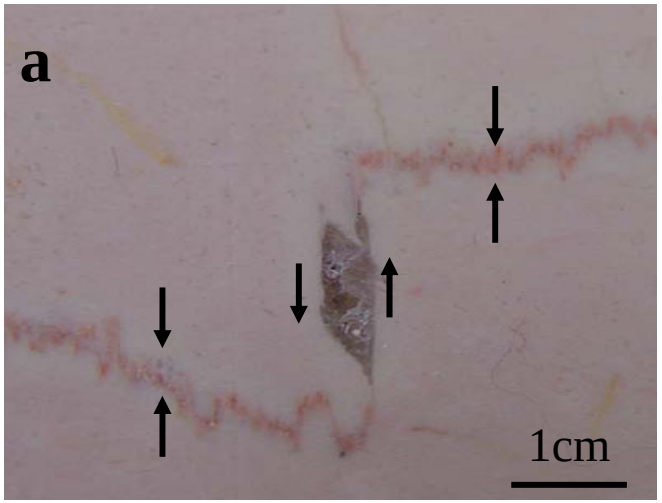

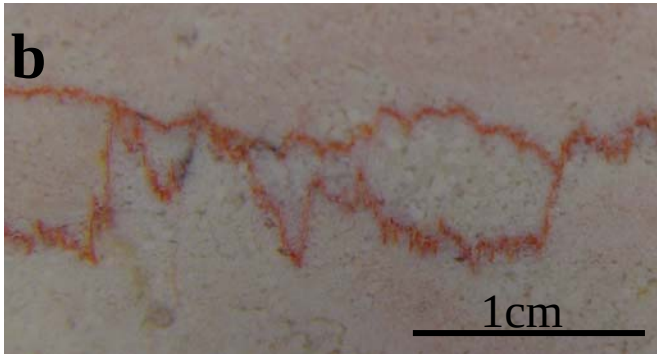

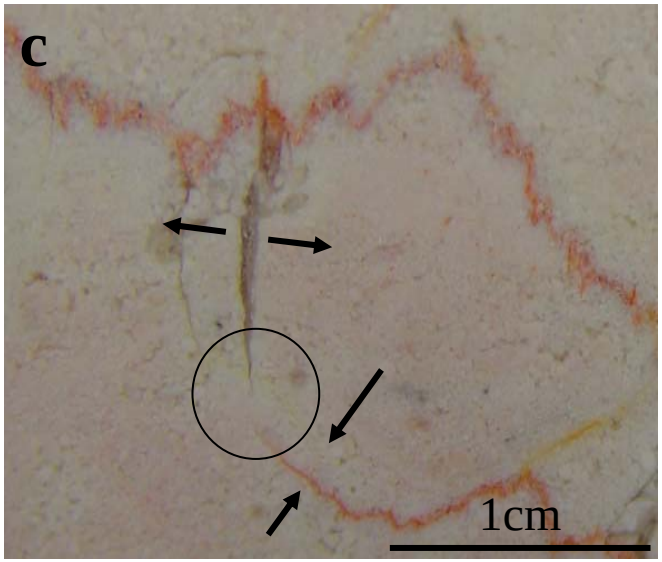

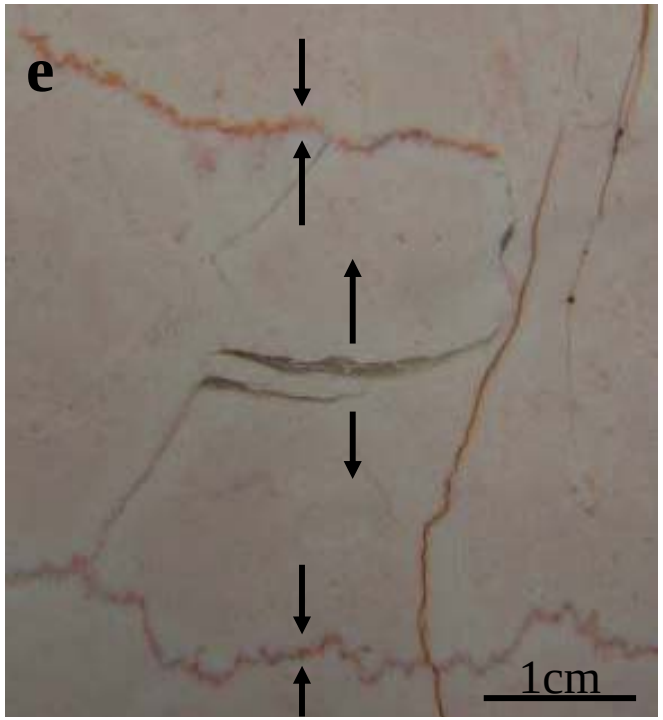

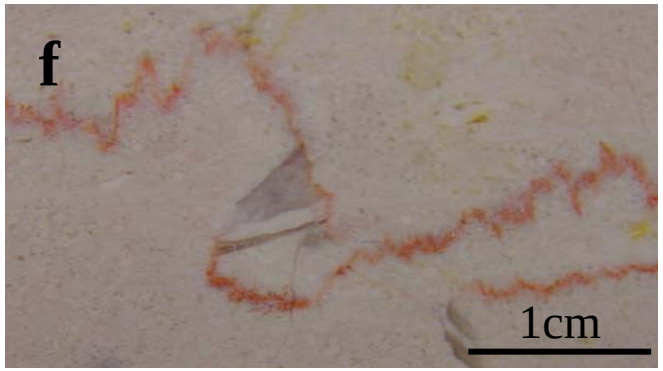

Fig 9: Zoom-in on the slab of Fig 4 showing small-scale field-relations between fractures and stylolites and between the stylolites themselves.

(a) Mode II fracture with pull-apart structure filled with cement connecting two stylolites. Interpreted strain direction is marked by arrows.

(b) Interconnected stylolite network that seems to be derived from stylolite "cannibalism" (see text for further explanation).

(c) Mode 1 veins sub-parallel to the stylolite teeth and splaying from them. The veins are commonly triangular, with the aperture being largest close to the stylolite surface. stylolite mean direction is changed near a vein (circled region).

(d) Complex connection between non-overlapping stylolites by an array of oblique veins.

(e) Veins parallel to stylolite surface mean direction indicating on extension that is in the same direction as compression (see arrows). This population of fractures parallel to stylolites is statistically common (see Fig 8).

(f) Vein and stylolites closely interacting. We interpret such intimate geometries as indicating on these features to be syn-formational.

Figs 9a, 9b and 9c illustrate possible mechanisms for the formation of the observations in Figs 8a, 8b and 8c, respectively.

Veins parallel to the mean surface of the stylolite are seen in Figs 9e, and are statistically important (Fig 8). Explanations and implications of this observation are suggested in the discussion.

4. Discussion

We suggest using natural divisions provided by percolation theory, in order to characterize the connectivity of natural stylolite populations. Pervious classification schemes for stylolites and pressure solution addressed roughness, spacing, relation to bedding and seam geometry (Park and Schot, 1968, Alvarez et al., 1978, Powell, 1979, Guzzetta, 1984, Engelder and Marshak, 1985, Railsback, 1993). Although these are very useful quantification approaches for classifying single stylolites, they do not address quantification needs for describing connectivity, as percolation theory offers.

Based on the observations and measurements presented above and on the theoretical possibilities for connectivity/percolation of surfaces in a 3-D space (presented in the introduction), we may categorize sedimentary stylolite populations into three connection/percolation geometries (Fig 10):

Class I: Isolated stylolite populations - no percolation of stylolites (Fig 10a):

These are stylolitic surfaces with clear terminations and no connections to other stylolites or fractures. Stockdale (1922) and Mardon (1988) report finding isolated stylolites and solution seams, respectively, in carbonates. Benedicto and Schultz (2010) investigated isolated tectonic stylolites and the strain associated with them in a ~0.2m-thick limestone layer in a fault-damage zone. Nenna and Aydin (2011) describe isolated tectonic solution seams in a sandstone formation.

a) Isolated stylolites *(zero connectivity)*

b) Long bedding-parallel stylolites *(2D connectivity)*

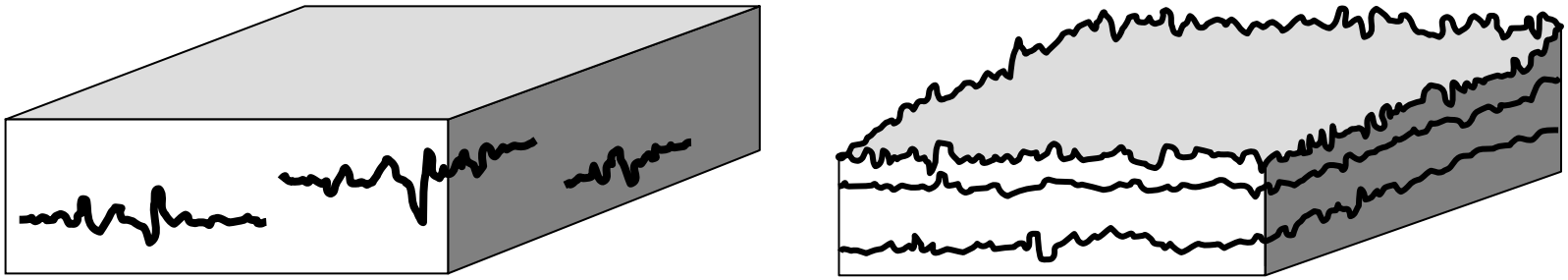

c1) Anastomosing stylolite network *(3D connectivity)*

c2) Stylolite-fracture network *(3D connectivity)*

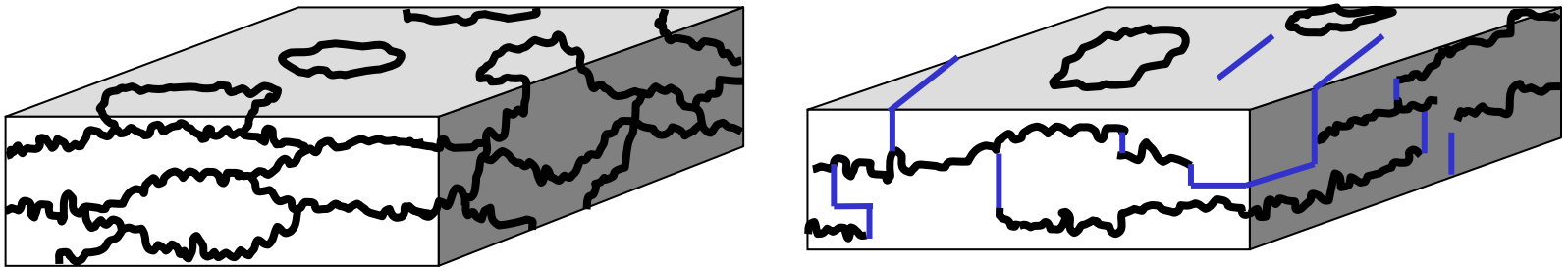

Fig 10. Connectivity-based classification of sedimentary stylolite populations: (a) Isolated stylolites; (b) Long bedding-parallel stylolite population; and (c) Interconnected-network stylolite population, further divided into (c1) anastomosing networks of stylolites and (c2) interconnected networks of stylolites and fractures (fractures appear in blue).

Class II: Long, bedding- parallel, stylolite populations - 2D percolation of stylolites (Fig 10b):

In this group stylolites are virtually infinite bedding-parallel rough surfaces that do not connect since they are parallel. These stylolitic surfaces have roughness with amplitude smaller than the spacing between them, so they also don't overlap. Tracing these surfaces connects the rock body from side-to side in 2 dimensions, sub-parallel to bedding, but not in the 3rd dimension, perpendicular to the surfaces and to bedding. Long bedding-parallel stylolites (or solution seams) were seldom described in the literature (Park and Schot, 1968, Safaricz, 2002, Safaricz and Davison, 2005).

Class III: Interconnected stylolite networks- 3D connectivity (Fig 10c):

Here stylolite surfaces are connected to one another by anastomosing or via fractures and veins. One can trace along these surfaces, following a "stylolite pathway", from any side of the rock to any other side, since surfaces percolate in 3 dimensions. Interconnected stylolite networks can be further divided into ***anastomosing stylolite networks*** and ***stylolite-fracture networks***. Interconnected stylolites were reported in several references (Mardon, 1988, Rye and Bradbury, 1988, Peacock and Sanderson, 1995, Smith, 2000, Safaricz, 2002, Eren, 2005).

The stylolite populations in our investigated sites either clearly fall into one of the 3 end-member connectivity classes, or present a combination of more than one class. ***Long, parallel stylolite populations*** (Fig 10b) and ***Interconnected networks*** (Fig 10c) are both commonly observed in field locations, as seen in the Supplementary Material (sites # 4-16). ***Isolated stylolites*** (Fig 10a) were not observed as a separate class in our field sites. Several stylolites in the stylolite-fracture network in the Umbria-Marche slab seem to terminate in our observed 2D plane, but possibly they are connected in 3D. The last site reported in the Supplementary (#17) is the only location with isolated features (often forming networks) and for this reason we included it, although the features are solution seams and not stylolites. Based on our fieldwork and on

371 literature, it appears that isolated stylolites are uncommon, though isolated pressure solution
372 seams are not rare (Mardon, 1988, Nenna and Aydin, 2011). In terms of evolution, isolated
373 stylolites, the non-percolating structure, may only be an intermediate stage in the evolution
374 process of percolating stylolites (which might explain their scarcity), as discussed in the next
375 sub-section. But in terms of topology isolated stylolites are one of the 3 topological possibilities
376 for connectivity of stylolitic planes, so for the sake of characterizing morphology we propose to
377 consider them as a separate class – the class of "no connectivity".
378 The Supplementary Material presents 14 additional field sites with large-scale stylolite
379 exposures. Out of these, 3 have long-parallel stylolite populations, 6 have interconnected
380 networks of both sub-groups, while 4 sites present a combination of end-member connectivities.
381 Combinations were mostly of long parallel stylolites with anastomosing network in between.
382

383 ### *4.1 Conceptual model for formation of observed stylolite populations*

384 Here we present a conceptual model of stylolite population formation to facilitate an
385 understanding of strain accommodation by stylolite populations. We review briefly the formation
386 of isolated and long-parallel stylolites, as it is discussed and modeled in detail in Aharonov and
387 Katsman (2009) and Laronne Ben-Itzhak et al. (2012), respectively. Table 2 summarizes how our
388 field measurements support suggested formation mechanisms for each of the different
389 populations.
390

391 #### ***4.1.1. Isolated stylolites:***

392 The amount of discussion of the formation of this type of population (Fletcher and Pollard,
393 1981, Mardon, 1988, Aharonov and Katsman, 2009) is inversely proportional to their prevalence.
394 These constitute Localized Volume Reduction (LVR) defects, as defined by Katsman and
395 Aharonov (2005), and Katsman et al. (2006a, b). Field observations of these features show

Table 2: Summary Table: suggested mechanisms for evolution of the various stylolite populations and the type of measurements that support each mechanism

Population Type	Suggested Mechanisms	Measurements	How Measurement Supports Mechanism
Isolated stylolites; zero connectivity	Initiation from seed, continuing dissolution and elongation due to both stress and composition (clay?)	A_{max} versus Length	If more developed (large A_{max}) in center and less towards edges, may indicate in-plane-propagation.
Long-Parallel stylolites; 2D connectivity	Initiation and continuation of roughening and dissolution on an existing surface (of higher clay content?)	-A_{max} versus Length -Spacing versus length - Surface roughness	Constant A_{max}, constant spacing between stylolite pairs along the surface, and upper cutoff to self-affinity suggest roughening of an existing surface.
Anastomosing stylolite networks; 3D connectivity	Cannibalism of bedding-parallel stylolites AND/OR Joining of isolated stylolites	-Intersection angle -Island dimensions	Finding of intersection angle of 35º-45º may support formation by joining of isolated stylolites; If angle is random – supports cannibalism. If around 90º, supports connection by fractures Understanding how to use the statistical characteristics of Islands to estimate the amount of dissolution, depends on the physics of network formation (discussed in the text)
Stylolite-fracture network; 3D connectivity	Increased shear-stress near stylolite tips AND/OR Connection of stylolite tips with Mode I cracks	-Directions (angles of stylolites and of fractures) -Small-scale field relations	Pull-aparts adjacent to stylolite tips Mode I cracks seem to attract stylolite tips.

References which appear in Table 1

1. Safaricz, M., *Pressure solution in chalk.* 2002, Royal Holloway University of London.
2. Arzani, N., *Stylolite networks in dolomitized limestones and their control on polished decorative stones: a case study from the Upper Cretaceous Khur quarries, central Iran.* JGeope, 2011. **1**(2): p. 25-37.
3. Losonsky, G., *Burial depth and lithofacies control of stylolite development in the Mississippian Salem Limestone, Illinois Basin*. 1992, University of Cincinnati.
4. Mardon, D., *Localized pressure solution and the formation of discrete solution seams.* 1988, Texas A&M University.

396 geometrical characteristics similar to cracks: (1) their amplitude and thickness taper towards their
397 edges and (2) their length increases with increasing seam thickness and amplitude (Stockdale,
398 1922, Mardon, 1988). Such features may develop self-similarly from an initial seed defect,
399 provided that it grows laterally sub-parallel to its plane and experiences continued dissolution on
400 its flanks (e.g. Fletcher and Pollard (1981)). Aharonov and Katsman (2009) show that
401 development of isolated stylolites can be explained by a feedback that arises when both clay
402 (present in the rock at some small fraction, and in initially higher content in seed defects) and
403 pressure solution enhance the dissolution process. Nenna and Aydin (2011) suggest that they
404 elongate and thicken due to the presence of asperities.
405
406 ***4.1.2. Long, parallel stylolite populations:*** The formation of this abundant, yet rarely
407 acknowledged, population type was indirectly studied before: the group of Ebner and Kohen
408 (Renard et al., 2004, Schmittbuhl et al., 2004, Koehn et al., 2007, Ebner et al., 2009a, Ebner et
409 al., 2009b) studied roughening from a prescribed surface. We suggest long parallel stylolites
410 form on planes where dissolution is for some reason enhanced, possibly due to initial chemical
411 heterogeneity (e.g. higher initial content of clay or other dissolution enhancing chemical
412 heterogeneity). In sedimentary stylolites such planes are most commonly bedding planes. Our
413 conceptual model suggests that long parallel stylolites do not evolve by lateral elongation of
414 isolated stylolites, but instead by dissolution-roughening on a preexisting plane, as suggested in
415 Laronne Ben-Itzhak et al. (2012). This is implied by the constant roughness amplitude we
416 measured along almost 1km (Fig 6), which does not follow the observed „parabolic' self-similar
417 profile of dissolution along isolated stylolites (Stockdale, 1922, Mardon, 1988). In
418 supplementary B we present a simple calculation that shows that the amount of dissolution on the
419 Blanche stylolites would have been far larger than measured if they evolved by elongation from a
420 seed rather than roughening of an existing surface. Spatially constant amplitude, as observed
421 here, is consistent with a process invariant under translation along the stylolite. It is easiest to

explain the observed long parallel stylolites as forming by localized dissolution on an initially flat plane (most often a bedding plane), that progressively roughens with time, driven by competing effects of stress, diffusion and noise (Koehn et al., 2012, Laronne Ben-Itzhak et al., 2012, Rolland et al., 2012). The dissolution creates a self-affine surface, following a scaling law between the out-of-plane root mean square width, *w(l)*, and the in-plane length, *l*, at which this width is defined: $w(l) \sim l^{H}$, with a Hurst exponent H~0.65, and with an upper cutoff for self-affinity that grows with increasing amount of dissolution (Renard et al., 2004, Schmittbuhl et al., 2004, Koehn et al., 2007, Ebner et al., 2009a, Laronne Ben-Itzhak et al., 2012).

4.1.3. Interconnected stylolite networks

This is again a very common type of population (sites # 2-6, 8-10, 13-16), which has not received much previous attention, and its formation has rarely been discussed. Based on our field observations, we propose that interconnected networks can form by one of three mechanisms or through a combination thereof. The three mechanisms are: (i) *Connection of tips of isolated stylolites* via dissolution or Mode II fractures; (ii) *Connection of stylolite tips with Mode I cracks* (iii) *Connection of long parallel stylolites;* (Figs 11a, 11b and 11c, respectively, linked to the examples in Figs 9a, 9b and 9c, respectively). In (i) and (ii) a population of non-touching surfaces of type (a) in Fig 10, connects as it evolves to finally create a percolating structure. In (iii) initially sub-parallel planes (type b in Fig 10) roughen enough with time to connect in the bedding perpendicular direction.

(i) Connection of tips of isolated stylolites: This may occur when two neighboring LVRs start to "feel" the normal and shear stress field of each other, and interact (e.g. Fueten and Robin (1992), Zhou and Aydin (2010)). Fig 11a shows a cartoon of normal and shear stresses that arise from dissolution on two horizontally over-lapping stylolites at a vertical distance *d* from each other, and the expected evolution due to these two stress fields, the normal and the shear:

448 **1.** ***Increased normal stress leading to increased dissolution*** (Fig 11a1): increased
449 compressive normal stress arises near the tip of each stylolite, with a maximum value achieved at
450 35º-45º from the mean stylolite plane, as indicated by the "heart-shaped" blue region, following
451 stress calculation for LVR. In case of uniform dissolution along the stylolite one can use the fact
452 that such an LVR defect induces a stress like an "edge dislocation" (Katsman et al., 2006a), and
453 use the calculated stress fields (Landau and Lifshitz (1986), p. 114) to conclude that maximum
454 compressive stress is induced by the tip at 45º. In case of elliptical dissolution the maximum is
455 found numerically at 35º (Katsman (2010a)). If spaced at a close enough vertical distance, *d*,
456 stylolites are expected to induce pressure solution in the compressive stress-enhanced region
457 between them, and thus connect by dissolution. Similar stylolite connections, via curving tips,
458 were seen by Mardon (1988) in a partially connected network of solution seams. In the
459 anastomosing networks observed at the Mitzpe Ramon site, curving planes are abundant: at
460 scales larger than ~2cm, angles between connecting stylolites are small (approach zero - become
461 parallel), while at smaller scales they are ~80º (Figure 8a). It is important to note that we find no
462 peak in the probability function of angles around the expected value of 35º-45º. This suggests
463 that there might be another process controlling stylolitic connections, possibly formation of shear
464 or Mode-I fractures that link adjacent stylolites, or connection by „cannibalism' of long parallel
465 stylolites, as detailed below.
466 **2.** ***Increased shear strain region leading to connection of stylolites by a shear fracture***
467 (Fig 11a2): In addition to compressive stress, any LVR defect - like the analogous "edge
468 dislocation" - is calculated theoretically to induce shear stresses near its tip in the plane normal to
469 it (Landau and Lifshitz (1986), p. 114). The stresses are linearly proportional to the amount of
470 volume removal (in this case amount of dissolution), and decay as 1/distance from the tip. The
471 fact that shear stress is induced by a stylolite tip can also be understood intuitively: Two
472 offsetting stylolites may be viewed as analogs to offset mid-ocean ridges, but with an opposite
473 sign. While mid-ocean ridges are spreading centers that create rock, stylolites are converging

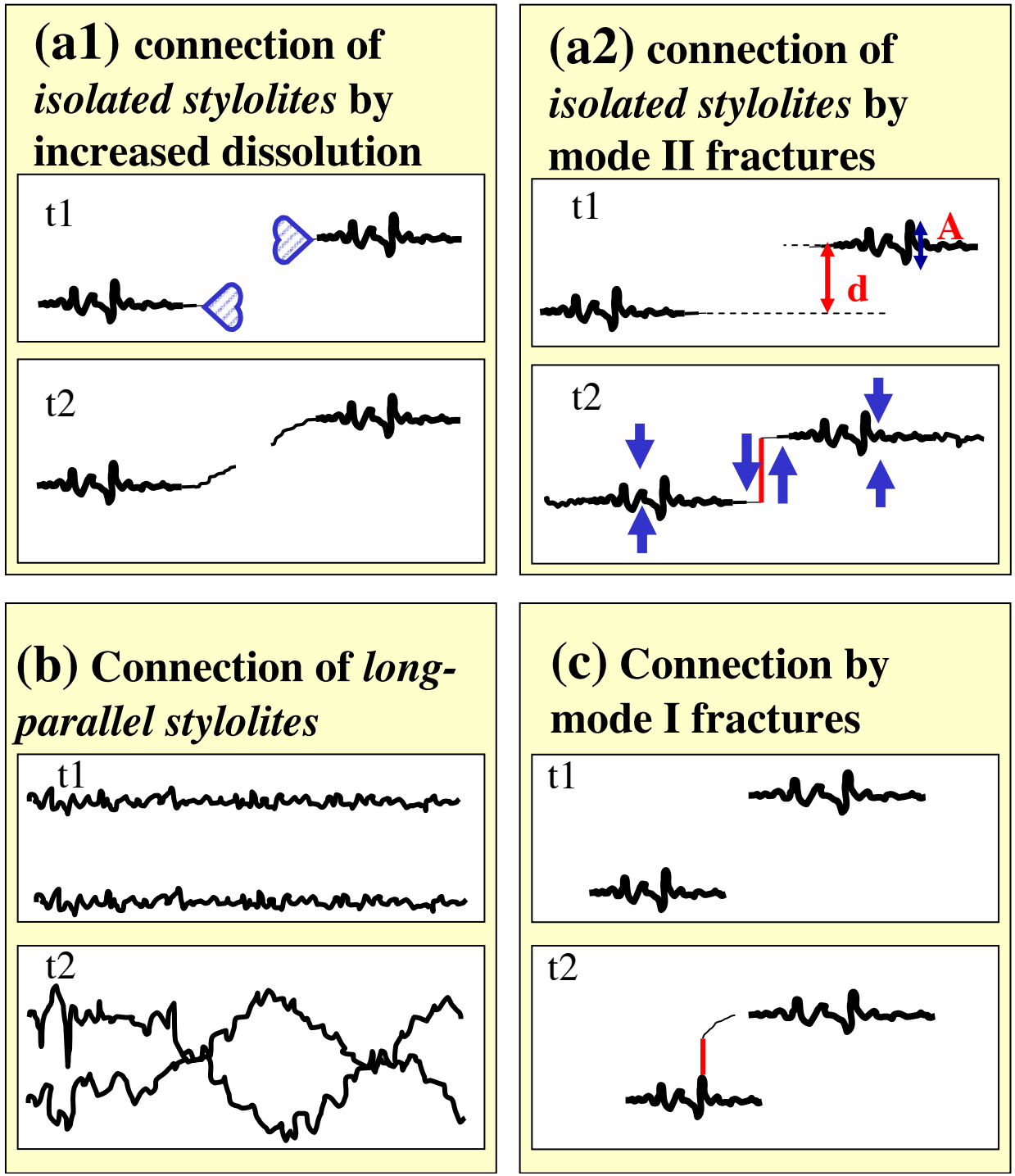

Fig 11:
Cartoon showing several possible mechanisms for the formation of interconnected stylolite networks from time t1 to t2.
(a) *Connection of isolated stylolites*. Increased normal stress (in blue-heart-shaped-regions) enhances dissolution and may change propagation direction (a1), while increased shear strain may cause fracturing (a2). This depends on the mechanical properties of the rock at that time. A and d (a2) control weather there will be connection by linkage or fracturing. Blue arrows (a2) show stress direction.

(b) *Connection of long-parallel stylolites* by their dissolution and roughening ("cannibalism" of closely spaced long-parallel stylolites).

(c) *Connection of stylolites via mode I fractures*, emanating from stylolite teeth. Such fractures can connect stylolites according to both models (a) and (b) (connection of single stylolites or continued dissolution of parallel stylolites). Tips of an adjacent stylolite may curve towards such vein, which induces extensive strain. This scenario fit with stylolite localizing via high

centers that destroy/dissolve rock (Peacock and Sanderson, 1995). When spreading/converging centers are positioned at an offset, they produce shear strain between them, proportional to the amount of rock created/destroyed. When the shear stress exceeds the material strength, a transfer fault will form and connect the two stylolites, similar to transform faults that connect offsetting mid-ocean ridges. "Pull-aparts" are common features in these transfer/transform faults, as seen in Fig 9a and discussed by Peacock and Sanderson (1995).

Two competing processes thus occur between "properly" oriented offset neighboring growing stylolites: shear fracturing between them due to increased shear stress, and dissolution due to increased normal stress. The two types of network stylolite populations (interconnected stylolites and stylolites and fractures) differ in the dominant mechanism: when shear fracturing dominates, stylolites and fractures will form; when dissolution dominates, interconnected stylolites form. Whether one mechanism prevails over the other may be associated with the hydrological state of the rock at the time of deformation: dissolution requires water at the grain contacts and a fluid path for solute to migrate or diffuse through. Alternatively, the control on which mechanism dominates may be related to the mechanical strength of the rock at the overlapping region, which in turn is controlled, *inter alia*, by rock composition, porosity and local defects.

(ii) Connection of stylolite tips with Mode I cracks **(Fig 11b)**: The ~~2~~ 2nd process by which isolated or planner stylolites may form networks, involves interaction between a stylolite and a Mode I vein. Mode I veins are often associated with stylolites (Rye and Bradbury, 1988, Smith, 2000, Eren, 2005) and several mechanisms have been suggested to explain their common appearance perpendicular to compression, i.e. at 90 degrees to stylolites (e.g. Fig 9b, 9d): concentrated compressive stress at tips of stylolite teeth (Zhou and Aydin, 2010); high fluid pore pressure within stylolites (Eren, 2005); and extensional stress in the mid-section of stylolites (Katsman, 2010). Regardless of its formation mechanism, a vein will impact stress-enhanced

500 dissolution in its vicinity, both by enhancing fluid-mediated solute transport (via flow and/or
501 diffusion), and by perturbing the stress field (Renard et al., 2000a, Renard et al., 2000b).
502 According to the stress fields (Landau and Lifshitz (1986), p. 114) both opening and Mode II
503 fractures are expected at certain regions around a stylolite tip, but 180^{o} between stylolites and
504 veins is not expected from the stress fields, since compactive features such as stylolites induce
505 compressive stress perpendicular to their plane (Fletcher and Pollard, 1981, Katsman et al.,
506 2006a) while veins induce exactly the opposite- extension perpendicular to their opening
507 direction.

508 Stress fields alone may thus not suffice to explain all vein -stylolite attraction, e.g. such as
509 the interaction in Fig 9b. It is possible to attribute some of the attraction to connectivity and
510 availability of fluid in veins, that allows fluid enhanced dissolution to dominate the location and
511 direction of stylolite propagation (e.g. (Renard et al., 2000a, Renard et al., 2000b, Aharonov and
512 Katsman, 2009). This suggests that the connectivity of stylolites and their ability to transfer
513 solute in fluid may dominate, at least in some cases, their growth and propagation. The fact that
514 fluid flow pathways, specifically cracks, enhance pressure solution rates has been observed also
515 in experiments (Gratier et al., 2009, Croize et al., 2010).
516
517 ***(iii) Connection of long parallel stylolites*** is the third possibility for formation of
518 interconnected stylolite networks (Fig 11c). Continued dissolution and roughening of essentially
519 2D stylolites can result in two stylolites merging in the 3rd, bedding perpendicular, direction, at
520 least along a limited segment (e.g. Fig 9c). Islands in this case are formed as leftover untouched
521 regions between coalescing initially self-affine surfaces. In a somewhat similar physical picture
522 (fracture fronts), where self-affine surfaces „eat each other' (cannibalism) and by this merge in
523 places, it was shown that island-scaling is related to the Hurst exponent of the merging surfaces
524 (Maloy et al., 2005, Maloy et al., 2006, Tallakstad et al., 2011). Comparison between the scaling
525 of islands and the Hurst exponent of the stylolites may aid in constraining the physical process

for network growth, and in understanding why the power-law relating out-of-plane and in-plane dimensions of islands is characterized by an exponent $\alpha \approx 0.67$, similar to the Hurst exponent of single stylolites, as reported e.g. by Ebner et al. (2009a); Koehn et al. (2007); Laronne Ben-Itzhak et al. (2012); and Rolland et al. (2012).

Connection angles could be used to distinguish whether connectivity occurred by isolated stylolites meeting at tips or via long stylolites "cannibalizing" each other: If stylolites are infinite- long- roughening- planes cannibalizing each other, connection angles are expected to be random, since the geometry of a stylolite at any given point (away from its tip) can be assumed to be independent of the geometry of the stylolites above and below it at the merging point. Alternatively, if stylolites connect at tips, connection angles are expected to be ~35º-45º if connection is by dissolution (Katsman, 2010), or ~90˚ if by a series of micro-fractures or by larger-scale fractures (Kaduri, 2013). In our case-studies connections are close to 90º at small scales, but present a large variability around this value (inset in Fig 7a), which suggests that micro-fractures are probably involved yet that both mechanisms are plausible.

4.2 Strain accommodated by stylolite networks

The dissolution on stylolites introduces an irreversible volume loss in the direction perpendicular to the stylolite, which produces a compactive strain. In the section below we attempt to determine the amount of strain accommodated by the three types of stylolite connectivity classes. The large-scale connections between stylolites and veins are shown to be important in allowing strain accommodation.

Isolated stylolites populations

Isolated stylolites can accommodate a finite and small amount of dissolution before connecting by dissolution or by shear fractures. Thus, although isolated stylolites may be

551 considered a distinct population in terms of their connectivity and percolation behavior, they are
552 most likely an intermediate feature in terms of strain. Isolated stylolites most likely eventually
553 develop into an anastomosing network. The evolutionary picture is expected to be complex since,
554 assuming that stylolite growth is solute-transfer-limited (as suggested by vein-tips attracting
555 stylolite-tips in this study, and as seen in some experiments, e.g. Renard et al. (2000b), Zhang
556 and Spiers (2005) and Zubtsov et al. (2005), Gratier et al. (2009)), then lack of connectivity at
557 initial stages slows growth of isolated stylolites relative to connected ones. This can explain the
558 scarcity of observations of isolated **well-developed** stylolites, while pressure solution seams,
559 which are often considered "baby- stylolites", are indeed found in isolated populations (Mardon,
560 1988, Nenna and Aydin, 2011).
561
562 ***Long, parallel stylolite populations***
563 Dissolution starts on an initially flat plane, which is most often a bedding plane that
564 progressively roughens with time. The roughness is self-affine and the upper cutoff for self-
565 affinity grows with time (e.g. Ebner et al. (2009a); Koehn et al. (2007)). The amount of
566 dissolution, *U,* is often estimated from maximum teeth height, A_{max}, but can also be estimated
567 from other statistical parameters of the surface (Laronne Ben-Itzhak et al., 2012), provided these
568 are measured on scales greater than the upper limits of this self-affinity. Estimates derived from
569 scales smaller than the upper limit for self-affinity (~50cm in the Blanche stylolites)
570 underestimate dissolution. Compactive vertical strain is calculated from the average amount of
571 dissolution on stylolites, $<U>$, and the average spacing between neighboring stylolites $<d>$,
572 according to: $\varepsilon_v = \frac{<U>}{<d>}$ The amount of dissolution, *U*, can also be estimated from seam
573 thickness (e.g. Tada and Siever (1989)) assuming that initial clay content was uniform, a
574 questionable assumption if dissolution started on a clay rich bed (Heald, 1955, 1956, Engelder
575 and Marshak, 1985, Marshak and Engelder, 1985, Aharonov and Katsman, 2009).

576

577 ***Anastomosing stylolites***

578 Strain in a section containing this type of stylolite population may be measured in one of two
579 ways, as from the long parallel stylolites: either from their seam thickness or from their statistical
580 characteristics. Yet understanding how to use the statistical characteristics (such as Fig 7) to
581 estimate the amount of dissolution, depends on the network formation which was discussed
582 above (Aharonov et al., 2010, Aharonov et al., 2011).

583

584 ***Stylolite-fracture networks***

585 Strain in this network is shared between the stylolites and the fractures, with Mode I and
586 Mode II fractures taking different roles. Similar to their large-scale analog, mid-ocean ridges,
587 **Shear fractures** have an important role in accommodating the compaction strain, even on the
588 scale of a basin. Pull-aparts can be used here to estimate the compactive strain.

589 **Opening veins** play a more complicated role. Veins appear in two main directions, parallel
590 and perpendicular to the main compression (Fig 8). The opening veins perpendicular to the
591 stylolites (as discussed above) play an important, though indirect, role in compaction, by
592 allowing fluid flow pathways and promoting rapid dissolution and compaction. In contrast,
593 examples for local extensional strain features found in a direction *parallel to the general*
594 *compaction direction* are shown in Fig 9e and also evident by the statistically significant
595 population of stylolite-parallel Mode I fractures (Fig 8). There may be several explanations for
596 these horizontal veins, and the understanding is made complicated by the fact that we do not
597 know the timing of the fractures: If they are coeval with the stylolites, they may have developed
598 due to small block rotations during the development of the stylolites, or due to local extensive
599 strain. Some wing-crack fractures may also have developed at a different time than the stylolites,
600 associated with a micro thrust fault under the effect of a tectonic horizontal contraction. Time
601 scales may also be different for the two processes: fracturing may be a fast process, while

602 pressure solution a slow one. This difference in timescales is also very interesting to study.
603 However, since we do not have any information on the tectonic context of this slab (the exact
604 location of the quarry from which it was taken is unknown), we cannot have more than these
605 speculations.
606

607 ### *4.3 Stylolites and fluid flow*

608 The effects of stylolites on flow have been discussed previously (Wong and Oldershaw,
609 1981, Carozzi and Vonbergen, 1987, Rye and Bradbury, 1988, Tada and Siever, 1989, Finkel
610 and Wilkinson, 1990, Raynaud and Carrioschaffhauser, 1992, Corwin et al., 1997, Ehrenberg,
611 2006, Heap et al., 2014). Yet the question of their connectivity, which is crucial for fluid flow,
612 has not been discussed. Two very different aspects are important with regards to fluid flow. The
613 first is the interaction between fluid-flow and stylolites **during** their formation; while the second
614 is the influence of stylolite populations on fluid flow in the crustal rocks in which they are
615 present, long **after** their formation. We address both aspects here, as we believe that the approach
616 presented in this paper is an important step in their understanding.
617

618 #### *4.3.1 Interaction between fluid-flow and stylolites during their formation*:

619 Fractures were shown to be intimately related to stylolites in the Umbria-Marche slab
620 (Fig 9). Some Mode I cracks are clearly formed with the stylolites (Figs 9a, 9b and 9f) while
621 others are less clearly timed (Figs 9d and 9e). Mode I fractures that seem coeval with the
622 stylolites have affected the growth of stylolites by diverting their average plane direction (Figs
623 9b1 and 9b2). This interaction could perhaps be explained if their presence enhanced solute
624 transport rates and also extended the volume available for precipitation of the dissolved matter,
625 before they were filled with precipitation. Stylolites probably also affected fracture formation, as
626 indicated by the latter originating from stylolite teeth, from the tapering of fractures away from

627 stylolites, and from shear fractures connecting stylolites. Therefore stylolites and fractures have a
628 mutual effect on each other in our case study. This symbiosis affects simultaneously the amount
629 of compactive strain that may occur in the system (see section 4.2), the pattern of fluid flow in
630 the system, and the locations of dissolution and precipitation. In a system containing very little or
631 no fractures (such as the long-parallel stylolites in the Blanche cliff), at least part of the
632 precipitation of the dissolved matter on the stylolites occurred in the adjacent porosity (as shown
633 in thin-sections in Laronne Ben-Itzhak et al. (2012)). In that site, measurements suggested a
634 scenario whereby the dissolution-precipitation process may have stopped once this porosity was
635 occluded, so that shutting down precipitation or diffusion in pores limited the amount of
636 dissolution that occurred (Laronne Ben-Itzhak et al., 2012). However, in a system that contains
637 many fractures, and could also be considered an open system, there is less constraint on the
638 amount of dissolution-driven compactive strain the system can undergo.
639
640 ***4.3.2 Interaction between fluid-flow and stylolites after their formation***:
641 Different percolation geometries of stylolites are each accompanied by associated
642 percolation geometries of the host rock: zero-connectivity of stylolites (isolated) comes together
643 with a fully percolated rock-body. 2D percolation of stylolites (long-parallel class) comes
644 together with parallel percolation of the rock-body between the stylolites but allows no
645 percolation in the bedding -perpendicular direction. 3D percolation of anastomosing networks
646 causes disconnected lenses of rock. It is important to recall that this percolation approach and the
647 division to stylolite connectivity-classes do not infer that stylolites are necessarily channels to
648 fluids. Stylolites may be of higher permeability than the rock-body regions between them (e.g.
649 Wong and Oldershaw (1981); Carozzi and Vonbergen (1987); ENREF_68 Carrio-Schaffhauser
650 et al. (1990); Raynaud and Carrioschaffhauser (1992); Heap et al. (2014);). But the opposite may
651 also exist in some cases: stylolites can be low-permeability features, due to the highly-cemented
652 regions often observed around stylolites (Corwin et al. (1997); Ehrenberg (2006)).

653 The connectivity is important both when stylolites act as flow conduits, and when they act as
654 barriers:
655 ***I: Isolated stylolites – no percolation:*** If stylolites have well defined tips and do not touch each
656 other, the system is below the percolation threshold, and their permeability shouldn't affect the
657 rock body too much, even if it is different than the permeability of the host rock.
658 ***II: Parallel stylolites - 2D percolation:*** These may induce anisotropic permeability. If they are
659 more permeable than the host rock permeability will be enhanced in the surface-parallel direction
660 but not in the perpendicular direction. Instead, if stylolites have lower permeability than the host
661 rock they will not affect the surface-parallel direction yet will act as barriers in the perpendicular
662 direction.
663 ***III: Stylolite Networks - 3D percolation:*** In this case the stylolites percolate but the rock body
664 lenses are disconnected from each other. Highly permeable stylolites will enhance flow in a more
665 or less isotropic manner, while low permeability stylolites will create a well-connected system of
666 barriers, expected to reduce permeability of the rock.
667

668 ## 5. Summary and conclusions

669 Our interest in large scale pressure solution structures, and fluid flow and strain in stylolitic
670 rocks, led us to suggest a classification of stylolite populations in the field, based on their
671 network connectivity. Fieldwork and percolation theory guided us to classify three distinct
672 groups: *isolated stylolites*, *long bedding-parallel stylolites* and *interconnected networks of*
673 *stylolites*. Isolated stylolites were previously quantified. The other two populations are quantified
674 here for the first time.
675 Measurements conducted to characterize very *long bedding-parallel stylolites* show that their
676 geometrical characteristics (e.g. maximum amplitude) are fairly constant along their length.
677 Observations reported here and in Laronne Ben-Itzhak et al. (2012) support a model of formation

678 by roughening caused by dissolution localized on preexisting planes, most often bedding planes,
679 (Renard et al., 2004, Schmittbuhl et al., 2004, Koehn et al., 2007, Ebner et al., 2009a). The
680 localization mechanism for uniform dissolution on very large bedding- planes is not strictly
681 known, but is likely connected to initial bedding-related compositional heterogeneity (possibly
682 higher clay content) (Lind, 1993), implying that stress may not be the only (nor the most
683 important) drive for their formation.

684 The interconnected networks of stylolites are further divided into *networks of anastomosing*
685 *stylolites* and *stylolites-fracture networks. Networks of anastomosing stylolites* show islands,
686 with a self-similar shape, bounded by stylolite seams. Connection angles between stylolites in the
687 network average ~90 degrees near the meeting point, while stylolites become parallel at larger
688 scales. The *Interconnected networks of stylolites and fractures*, which are composed of both
689 Mode I and II fractures connecting stylolites, show that most fractures are perpendicular to
690 stylolites. The measurements on both types of interconnected networks, together with small-scale
691 observations of field relations between stylolites and fractures, suggest the possibility of several
692 formation mechanisms for stylolite networks: (1) connection of tips of active isolated stylolites;
693 (2) connection (via cannibalization) of long parallel stylolites; and (3) connection of stylolite tips
694 with Mode I cracks. However full understanding of these mechanisms and when each one
695 operates needs further work.

696 The measurements and analysis presented in this manuscript have several important
697 implications. The first is that stylolites may form by various mechanisms. This is implied from
698 the recognition that there are different geometries with different characteristics of stylolite
699 populations. In some cases stylolites may propagate laterally during dissolution, while in others
700 the in-plane distribution is set from the beginning. A second conclusion is that stylolites and
701 veins often co-exist in a geometry which indicates that they interact with one another. Stylolites
702 may induce stress perturbations that govern the location of fractures (emanating from their teeth
703 or edges). Fractures affect stylolites (by diverting their mean direction) possibly due to the

704 increased solute transport that they allow. The two processes may have widely different time
705 scales –fractures are often fast while stylolites dissolve slowly. The intriguing interactions affect
706 both the strain and the fluid flow pathways, although quantification and full understanding need
707 further field, modeling, and lab work.
708

Acknowledgments

This research was sponsored by ExxonMobil and by an ISF grant #751/08. We deeply thank Yehuda Eyal, Eitan Sass and the late and beloved Hagai Ron, for sharing with us their knowledge and experience in the field, and for showing us many of the field locations. EA and RT acknowledge the support of the Marie Curie ITN Flowtrans.

Figure Captions

Figure 1: Long parallel stylolites in the Blanche cliff, Northern Israel (adapted from Figure 1 in Ben-Itzhak et al. (2012)).
(a) Part of the cliff with four stylolites (labeled „4(19)', „5(7)', „5(9)' and „5(13)' in Figure 5b) marked in red, showing they can be traced for a large distance.
(b) Zoom on two other stylolites („3(10)' marked by a green arrow, and „3(11)', see Figure 5b), where stylolite cm-scale roughness is evident.

Figure 2: Interconnected stylolite network from a Cenomanian limestone quarry near Mitzpe Ramon, Southern Israel (site 2, Table 1).
(a) Large scale photo and **(b)** zoom of the mapped exposure, studied from two perpendicular sides. High-resolution photographs were combined using a grid for digitization of the stylolite network (the black grid in (a) was drawn on the photo to illustrate where the actual grid on the exposure was marked). 5.5 x 1.2 m^2 were mapped on either of the two perpendicular sides.

Figure 3: Three scales of a digitized map of the interconnected stylolite network seen in Figure 2 (the right section of the two perpendicular exposures in Figure 2). Regions between connected stylolites are termed "islands", and are described by several parameters: island area S; connection angle θ between stylolite segments of length L; and a bounding rectangle with bedding-parallel and bedding perpendicular dimensions ξ_{II} and $\xi_{\perp}$, respectively.

Figure 4: Interconnected network of stylolites and fractures in limestone (Calcare Massiccio Formation, Jurassic, Italy).
(a) Close-up photo showing interacting stylolites and fractures; and
(b) Larger scale digitized map of major and minor stylolites (pink and green, respectively) and of fractures (blue).

Figure 5: Images showing the Blanche (Ein El-Assad Fm.) section in the northern part of the cliff, where all 65 stylolites were identified and measured.
(a) The section was divided to 9 major units differentiated by major stylolites (in orange). Most of the measurements were performed in the parts that are marked in white (these are the same units as in the orange-part but on a closer and more accessible cliff).

(b) Zoom on rectangle in (a). Stylolites are labeled according to their vertical position within a unit, i.e., 5(3) is the third stylolite from the bottom of unit 5. Spacing between neighboring stylolites (5(12) and 5(13), as an example) is displayed in white.

Figure 6: Measurements conducted on long parallel stylolites at several locations along the ~1km – long Blanche cliff.

(a) Spacing between three couples of stylolites.

(b) and **(c)** Maximum teeth amplitude (A_{max}) of six different stylolites (viewed in two separate graphs only for purposes of convenience). Error bars are the standard deviation of several measurements in each location. No trend in spacing or A_{max} along the length of the stylolites is identified.

Figure 7: Statistical analysis on variables illustrated in Figure 3c, performed in Mitzpe Ramon quarry.

(a) angle between adjacent stylolites as function of distance from junction, $\theta(L)$, measured at all stylolite junctions. Each data point is the average of all $\theta(L_i)$ in the exposure, where i is the index of the junction. Error bars are standard deviation. Both are acquired from normal distribution functions produced for each L_i. The inset is such an example distribution for L=0.9cm.

(b) Island heights $\xi_{\perp}$ versus island width ξ_{II} measured on all islands in the outcrop, as explained in the text. The line is a best fit to the correlation between $\xi_{\perp}$ and ξ_{II}.

Figure 8: Orientations of stylolites and fractures in the Umbria–Marche slab, Apennines (analyzed upon map in Fig 4b).

H indicates horizontal (bedding parallel) and V indicates vertical. Red indicates the stylolite population orientation and blue the fracture orientations.

Figure 9: Zoom-in on the slab of Figure 4 showing small-scale field-relations between fractures and stylolites and between the stylolites themselves.

(a) Mode II fracture with pull-apart structure filled with cement connecting two stylolites. Interpreted strain direction is marked by arrows.

(b1) and **(b2)** Two examples of Mode 1 veins sub-parallel to the stylolite teeth and splaying from them. The veins are commonly triangular, with the aperture being largest close to the stylolite surface (b1). Stylolite mean direction is changed near a vein (circled regions).

781 **(c)** Interconnected stylolite network that seems to be derived from stylolite "cannibalism" (see
782 text for further explanation).
783 **(d)** Complex connection between non-overlapping stylolites by an array of oblique veins.
784 **(e)** Veins parallel to stylolite surface mean direction. This population of fractures parallel to
785 stylolites is statistically common (see Figure 8). The formation of these wing-crack fractures may
786 be explained in several ways (see discussion in text).
787 **(f)** Vein and stylolites closely interacting.
788 Possible mechanisms for the formation of the observations in Figures 9a, 9b and 9c, appear in
789 Figures 11a, 11b and 11c, respectively.
790
791 **Figure 10:** Connectivity/percolation-based classification of sedimentary stylolite populations: **(a)**
792 Isolated stylolites; **(b)** Long bedding-parallel stylolite population; and **(c)** Interconnected-
793 network stylolite population, further divided into (c1) anastomosing networks of stylolites and
794 (c2) interconnected networks of stylolites and fractures (fractures appear in blue).
795
796 **Figure 11:** Cartoon showing several possible mechanisms for the formation of interconnected
797 stylolite networks between times t1 and t2.
798 **(a)** *Connection of isolated stylolites*. Increased normal stress (in blue-heart-shaped-regions)
799 enhances dissolution and may change propagation direction (a1), while increased shear strain
800 may cause fracturing (a2). This depends on the mechanical properties of the rock at that time. *A*
801 and *d* (a2) control whether there will be connection by linkage or fracturing. Thick blue arrows
802 (a2) show stress direction.
803 **(b)** *Connection of stylolites via mode I fractures*, emanating from stylolite teeth. Tips of an
804 adjacent stylolite may curve towards such vein, which induces extensive strain. This scenario fits
805 with stylolite localizing via high dissolution rates. Rapid dissolution in diffusion limited systems
806 can be induced by rapid fluid pathways.
807 **(c)** *Connection of long-parallel stylolites* by their dissolution and roughening ("cannibalism" of
808 closely spaced long-parallel stylolites).
809

Reference List

Aharonov, E., Katsman, R. 2009. Interaction between Pressure Solution and Clays in Stylolite Development: Insights from Modeling. *American Journal of Science* **309**(7), 607-632.

Aharonov, E., Katsman, R., Laronne Ben-Itzhak, L. 2010. How do stylolite networks and stylolite-fracture networks form: insights from modeling. In: *28th IUGG Conference on Mathematical Geophysics*, Pisa, Italy.

Aharonov, E., Laronne Ben-Itzhak, L., Katsman, R., Karcz, Z., Kaduri, M. 2011. Stylolite Populations in Limestone: Field observations and formation models, Abstract T33C-2427. In: *AGU fall meeting*, San Francisco.

Alvarez, W., Engelder, T., Geiser, P. A. 1978. Classification of Solution Cleavage in Pelagic Limestones. *Geology* **6**(5), 263-266.

Andrews, L. M., Railsback, L. B .7997 .Controls on stylolite development: Morphologic, lithologic, and temporal evidence from bedding-parallel and transverse stylolites from the US Appalachians. *Journal of Geology* **105**(1), 59-73.

Benedicto, A., Schultz, R. A. 2010. Stylolites in limestone: Magnitude of contractional strain accommodated and scaling relationships. *Journal of Structural Geology* **32**, 1250-1256.

Bour, O., Davy, P. 1998. On the connectivity of three-dimensional fault networks,. *Water Resources Research* **34**(10), 2611-2622.

Bunde ,A., Havlin, S. 1991. Fractals and disordered systems (edited by Bunde, A. & Havlin, S.). Springer-Verlag New York, Inc., 350.

Carozzi, A. V., Vonbergen, D. 1987. Stylolitic Porosity in Carbonates - a Critical Factor for Deep Hydrocarbon Production. *Journal of Petroleum Geology* **10**(3), 267-282.

Carrio-Schaffhauser, E., Raynaud, S., Latière, H. J., Mazerolle, F. 1990. Propagation and localization of stylolites in limestones. *Geological Society, London, Special Publications* **54**(1), 193-199.

Cartwright, J .A., Trudgill, B. D., Mansfield, C. S. 1995. Fault growth by segment linkage: an explanation for scatter in maximum displacement and trace length data from the Canyonlands Grabens of SE Utah. *Journal of Structural Geology* **17**(9), 1319-1326.

Cello, G. 1997 .Fractal analysis of a Quaternary fault array in the central Apennines, Italy. *Journal of Structural Geology* **19**(7), 945-963.

Corwin, L. W., Broomhall, R. W., Saidikowski, R. M., Wooten, J. N. 1997. Stylolites Impact the Miscible Nitrogen Flood in a Mature Carbonate Oil Field. *SPE International, Inc.,* **37780**, 213-221.

Croize, D., Renard, F., Bjorlykke, K., Dysthe, D. K. 2010. Experimental calcite dissolution under stress: Evolution of grain contact microstructure during pressure solution creep. *Journal of Geophysical Research-Solid Earth* **115.**

Dawers, N. H., Anders, M. H., Scholz, C. H. 1993. Growth of normal faults - displacement-length scaling. *Geology* **21**(12), 1107-1110.

Deboer, R. B. 1977. Thermodynamics of Pressure Solution - Interaction between Chemical and Mechanical Forces. *Geochimica Et Cosmochimica Acta* **41**(2), 249-256.

Ebner, M., Koehn, D., Toussaint, R., Renard, F. 2009a. The influence of rock heterogeneity on the scaling properties of simulated and natural stylolites. *Journal of Structural Geology* **31**(1), 72-82.

Ebner, M., Koehn, D., Toussaint, R., Renard, F., Schmittbuhl, J. 2009b. Stress sensitivity of stylolite morphology. *Earth and Planetary Science Letters* **277**(3-4), 394-398.

Ehrenberg, S. N. 2006. Porosity destruction in carbonate platforms. *Journal of Petroleum Geology* **29**(1), 41-51.

Engelder, T., Marshak, S. 1985. Disjunctive cleavage formed at shallow depths in sedimentary rocks. *Journal of Structural Geology* **7**(3/4), 327-343.
Eren, M. 2005. Origin of stylolite related fractures in atoka bank carbonates, eddy county, New Mexico, USA. *Carbonates and Evaporites* **20**(1), 42-49.
Finkel, E. A., Wilkinson, B. H. 1990. Stylolitization as Source of Cement in Mississippian Salem Limestone, West-Central Indiana. *Aapg Bulletin-American Association of Petroleum Geologists* **74**(2), 174-186.
Fletcher, R. C., Pollard, D. D. 1981. Anti-Crack Model for Pressure Solution Surfaces. *Geology* **9**(9), 419-424.
Fueten, F., Robin, P. Y. F. 1992. Finite-Element Modeling of the Propagation of a Pressure Solution Cleavage Seam. *Journal of Structural Geology* **14**(8-9), 953-962.
Gratier, J.-P., Guiguet, R., Renard, F., Jenatton, L., Bernard, D. 2009. A pressure solution creep law for quartz from indentation experiments. *Journal of Geophysical Research: Solid Earth* **114** B03403.
Greene, G. W., Kristiansen, K., Meyer, E. E., Boles, J. R., Israelachvili, J. N. 2009. Role of electrochemical reactions in pressure solution. *Geochimica Et Cosmochimica Acta* **73**(10), 2862-2874.
Gruzman, Y. 1997. Origin of sedimentary stylolites from Israel. Unpublished M.Sc thesis, Hebrew University.
Gupta, A., Scholz, C. H. 2000. A model of normal fault interaction based on observations and theory. *Journal of Structural Geology* **22**(7), 865-879.
Guzzetta, G. 1984. Kinematics of stylolite formation and physics of pressure-solution process. *Tectonophysics* **101**, 383-394.
Heald, M. T. 1955. Stylolite in sandstones. *The Journal og Geology* **63**(2), 101-114.
Heald, M. T. 1956. Cementation of Simpson and St. Peter sandstones in parts of Oklahoma, Arkansas and Missouri. *The Journal of Geology* **64**(1), 16-30.
Heap, M. J., Baud, P., Reuschlé, T., Meredith, P. G. 2014. Stylolites in limestones: Barriers to fluid flow? *Geology* **42**(1), 51-54.
Hickman, S. H., Evans, B. 1995. Kinetics of Pressure Solution at Halite-Silica Interfaces and Intergranular Clay Films. *Journal of Geophysical Research-Solid Earth* **100**(B7), 13113-13132.
Kaduri, M. 2013. Interconnected Stylolite Networks: field observations, characterization, and modeling, M.Sc. thesis, The Hebrew University.
Kaplan ,M. Y. 1976. Origin of stylolites. *Docl. Acad. Sci USSR, Earth Sci. Sect.* **221**, 205-7.
Karcz, Z., Scholz, C. H. 2003. The fractal geometry of some stylolites from the Calcare Massiccio Formation, Italy. *Journal of Structural Geology* **25**(8), 1301-1316.
Katsman, R. 2010. Extensional veins induced by self-similar dissolution at stylolites: analytical modeling. *Earth and Planetary Science Letters* **299**, 33-41.
Katsman, R., Aharonov, E. 2005. Modelling localized volume changes: Application to pressure solution and stylolites. *Geochimica Et Cosmochimica Acta* **69**(10), A312-A312.
Katsman, R., Aharonov, E., Scher, H. 2006a. Localized compaction in rocks: Eshelby's inclusion and the Spring Network Model. *Geophysical Research Letters* **33**(10).
Katsman, R., Aharonov, E., Scher, H. 2006b. A numerical study on localized volume reduction in elastic media: Some insights on the mechanics of anticracks. *Journal of Geophysical Research-Solid Earth* **111**(B3).
Koehn, D., Ebner, M., Renard, F., Toussaint, R., Passchier, C. W. 2012. Modelling of stylolite geometries and stress scaling. *Earth and Planetary Science Letters* **341-34**.771-704 ,4
Koehn, D., Renard, F., Toussaint, R., Passchier, C. W. 2007. Growth of stylolite teeth patterns depending on normal stress and finite compaction. *Earth and Planetary Science Letters* **257**(3-4), 582-595.

909 Landau, L. D., Lifshitz, E. M. 1986. *Theory of Elasticity: Vol. 7 of Course of Theoretical*
910 *Physics*. Elsevier Ltd.
911 Laronne Ben-Itzhak, L., Aharonov, E., Toussaint, R., Sagy, A. 2012. Upper bound on stylolite
912 roughness as indicator for amount of dissolution. *Earth and Planetary Science Letters*
913 **3**.796-786 ,118–17
914 Lehner, F. K. 1995. A Model for Intergranular Pressure Solution in Open Systems.
915 *Tectonophysics* **245**(3-4), 153-170.
916 Lind, I. L. 1993. Stylolites in chalk from Leg 130, Ontong Java Plateau. *Proceedings of the*
917 *Ocean Drilling Program, Scientific Results* **130**, 445-451.
918 Main, I. 1996. Statistical physics, seismogenesis, and seismic hazard. *Reviews of Geophysics*
919 **34**(4), 433-462.
920 Maloy, K. J., Santucci, S., Schmittbuhl, J., Toussaint, R. 2006. Local Waiting Time Fluctuations
921 along a Randomly Pinned Crack Front. *Physical Review Letters* **96**(4), 045501.
922 Maloy, K. J., Toussaint, R., Schmittbuhl, J. 2005. Dynamics and structure of interfacial crack
923 fronts. In: *Proceedings of the ICF11, 11th International Conference on Fracture*, Torino.
924 Mardon, D. 1988 .Localized pressure solution and the formation of discrete solution seams.
925 Unpublished Ph. D. thesis, Texas A&M University.
926 Marshak, S., Engelder, T. 1985. Development of Cleavage in Limestones of a Fold-Thrust Belt
927 in Eastern New-York. *Journal of Structural Geology* **7**(3-4), 345-359.
928 McLachlan, D. S., Blaszkiewicz, M., Newnham, R. E. 1990. Electrical Resistivity of
929 Composites. *Journal of the American Ceramic Society* **73**(8), 2187-2203.
930 McLeod, A. E., Dawers, N. H., Underhill, J. R. 2000. The propagation and linkage of normal
931 faults: insights from the Strathspey-Brent-Statfjord fault array, northern North Sea. *Basin*
932 *Research* **12**(3-4), 263-284.
933 Nenna, F. A., Aydin, A. 2011. The formation and growth of pressure solution seams in clastic
934 rocks: A field and analytical study. *Journal of Structural Geology* **33**, 633-643.
935 Park, W. C., Schot, E. H. 1968. Stylolites - Their Nature and Origin. *Journal of Sedimentary*
936 *Petrology* **38**(1), 17797-5.
937 Paterson, M. S. 1995. A Theory for Granular Flow Accommodated by Material Transfer Via an
938 Intergranular Fluid. *Tectonophysics* **245**(3-4), 135-151.
939 Peacock, D. C. P., Sanderson, D. J. 1995. Pull-Aparts, Shear Fractures and Pressure Solution.
940 *Tectonophysics* **241**(1-2), 1-13.
941 Powell, C. M. 1979. A morphological classification of rock cleavage. *Tectonophysics*
942 *Microstructural processes during deformation and metamorphism* **58**(1-2), 21-34.
943 Railsback, L. B. 1993. Lithologic Controls on Morphology of Pressure-Dissolution Surfaces
944 (Stylolites and Dissolution Seams) in Paleozoic Carbonate Rocks from the Mideastern
945 United-States. *Journal of Sedimentary Petrology* **63**(3), 513-522.
946 Raynaud, S., Carrioschaffhauser, E. 1992. Rock Matrix Structures in a Zone Influenced by a
947 Stylolite. *Journal of Structural Geology* **14**(8-9), 973-980.
948 Renard, F., Brosse, E ,.Gratier, J. P. 2000a. The Different Processes Involved in the Mechanism
949 of Pressure Solution in Quartz-Rich Rocks and their Interactions. In: *Quartz Cementation*
950 *in Sandstones* (edited by Worden, R. H. & Morad, S.). Blackwell Publishing Ltd.,
951 Oxford, UK.
952 Renard, F., Dysthe, D., Feder, J., Bjorlykke, K., Jamtveit, B. 2001. Enhanced pressure solution
953 creep rates induced by clay particles: Experimental evidence in salt aggregates.
954 *Geophysical Research Letters* **28**(7), 1295-1298.
955 Renard, F., Gratier, J. P ,.Jamtveit, B. 2000b. Kinetics of crack-sealing, intergranular pressure
956 solution, and compaction around active faults. *Journal of Structural Geology* **22**(10),
957 1395-1407.

Renard, F., Schmittbuhl, J., Gratier, J. P., Meakin, P., Merino, E. 2004. Three-dimensional roughness of stylolites in limestones. *Journal of Geophysical Research-Solid Earth* **109**(B3).

Rolland, A., Toussaint, R., Baud, P., Schmittbuhl, J., Conil, N., Koehn, D., Renard, F., Gratier, J. P. 2012a. Modeling the growth of stylolites in sedimentary rocks. *Journal of Geophysical Research-Solid Earth* **117**(6), B06403.

Rye, D. M., Bradbury, H. J. 1988. Fluid-Flow in the Crust - an Example from a Pyrenean Thrust Ramp. *American Journal of Science* **288**(3), 197-235.

Safaricz, M. 2002. Pressure solution in chalk. Unpublished Ph.D. thesis, Royal Holloway University of London.

Safaricz, M., Davison, I. 2005. Pressure solution in chalk. *Aapg Bulletin* **89**(3), 383-401.

Schmittbuhl, J., Renard, F., Gratier, J. P., Toussaint, R. 2004. Roughness of stylolites: Implications of 3D high resolution topography measurements. *Physical Review Letters* **93**(23).

Segall, P., Pollard, D. D. 1980. Mechanics of discontinuous faults. *Journal of Geophysical Research* **85**(B8), 4337-4350.

Shimizu, I. 1995. Kinetics of Pressure Solution Creep in Quartz - Theoretical Considerations. *Tectonophysics* **245**(3-4), 121-134.

Sibley, D. F., Blatt, H. 1976. Intergranular Pressure Solution and Cementation of Tuscarora Orthoquartzite. *Journal of Sedimentary Petrology* **46**(4), 881-896.

Smith, J. V. 2000. Three-dimensional morphology and connectivity of stylolites hyperactivated during veining. *Journal of Structural Geology* **22**(1), 59-64.

Sneh, A., Weinberger, R. 2003. Geological Map of Israel. Sheet 2-II Metulla. Israel Geological Survey.

Stockdale, P. B. 1922. Stylolites: their nature and origin. *Indiana University Studies* **9**, 1-97.

Tada, R., Siever, R. 1989. Pressure Solution During Diagenesis. *Annual Review of Earth and Planetary Sciences* **17**, 89-118.

Tallakstad, K. T., Knudsen, H. A., Ramstad, T ,.Løvoll, G., Måløy, K. J., Toussaint, R., Flekkøy, E. G. 2009a. Steady-State Two-Phase Flow in Porous Media: Statistics and Transport Properties. *Physical Review Letters* **102**(7), 074502.

Tallakstad, K. T., Løvoll, G., Knudsen, H. A., Ramstad, T., Flekkøy, E. G., Måløy, K. J. 2009b. Steady-state, simultaneous two-phase flow in porous media: An experimental study. *Physical Review E* **80**(3), 036308

Tallakstad, K. T., Toussaint, R., Santucci, S., Schmittbuhl, J., Maloy, K. J. 2011. Local dynamics of a randomly pinned crack front during creep and forced propagation: An experimental study. *Physical Review E* **83**(4), 046108.

Thomson, A. 1959. *Pressure solution and porosity*. Soc. Econ. Paleontol. Mineral. Special publication.

Vermilye, J. M., Scholz, C. 1995. Relation between vein length and aperture. *Journal of Structural Geology* **17**(3), 423-434.

Walderhaug, O., Bjorkum, P. A., Aase, N. E. 2006. Kaolin-coating of stylolites, effect on quartz cementation and general implications for dissolution at mineral interfaces. *Journal of Sedimentary Research* **76**(1-2), 234-243.

Weyl, P. K. 1959. Pressure solution and the force of crystallization: a phenomenological theory. *Journal of Geophysical Research-Solid Earth* **64**, 2001-2025.

Willemse, E. J. M. 1997. Segmented normal faults: Correspondence between three-dimensional mechanical models and field data. *Journal of Geophysical Research -Solid Earth* **102**(B1), 675-692.

Wong, P. K., Oldershaw, A. 1981. Burial Cementation in the Devonian, Kaybob Reef Complex, Alberta, Canada. *Journal of Sedimentary Petrology* **51**(2), 507-520.

Zhang, X., Spiers, C. J. 2005. Compaction of granular calcite by pressure solution at room temperature and effects of pore fluid chemistry. *International Journal of Rock Mechanics and Mining Sciences* **42**(7-8), 950-960.
Zhou, X., Aydin, A. 2010. Mechanics of pressure solution seam growth and evolution. *Journal of Geophysical Research-Solid Earth* **115**, 18.
Zubtsov, S., Renard, F., Gratier, J. P., Dysthe, D. K., Traskine, V. 2005. *Single contact pressure solution creep on calcite monocrystals*. Geological society Special Publication.